Post-depositional evolution over a time scale of 1 million years of eastern Mediterranean organic-rich and organic-poor sediments: new insights on the debromination and layer-silicate markers

Anne Murat, Daniel Beaufort, Benoît Hebert, François Baudin, Stefano Bernasconi, Emmanuelle Ducassou, Céline Lelievre, Emmanuel Poizot, Maximilien Mathian, O. Grauby

1 Post-depositional evolution over a time scale of 1 million years of eastern

2 Mediterranean organic-rich and organic-poor sediments: new insights on the

3 debromination and layer-silicate markers

4 Evolution post-dépôt à l'échelle d'un million d'années de sédiments riches et pauvres

5 en matière organique en Méditerranée orientale: nouveaux aperçus sur la

6 débromination et les marqueurs argileux

7

8 Anne MURAT[1,2], Daniel BEAUFORT[3], Benoît HEBERT[3], François BAUDIN[4],

9 Stefano BERNASCONI[5], Emmanuelle DUCASSOU[6], Céline LELIEVRE[1],

10 Emmanuel POIZOT[1,2], Maximilien MATHIAN[3] and Olivier GRAUBY[7]

11 (1) Laboratoire universitaire des sciences appliquées de Cherbourg. Normandie

12 Univ., UNICAEN, LUSAC, 50100 Cherbourg, France

13 (2) Conservatoire National des Arts et Métiers. INTECHMER, 50100 Cherbourg,

14 France

15 (3) IC2MP UMR 7285, Université de Poitiers, 86073 Poitiers cedex 9, France

16 (4) iSTeP, UMR 7193, Université de Paris VI, 75005 Paris, France

17 (5) Geologisches Institut, ETHZ Zuerich, 8092 Zuerich, Switzerland

18 (6) UMR-CNRS 5805 EPOC, Université de Bordeaux, 33615 Pessac cedex, France

19 (7) UMR 7325 CINaM/CNRS, Université Aix-Marseille campus de Luminy, 13288

20 Marseille cedex 9, France

21 Email: anne.murat@cnam.fr

22

23 Key words: organic matter, clay minerals, bromine, eogenesis, sapropel,

24 Mediterranean sea

25   Mots clés : matière organique, minéraux argileux, brome, éogenèse, sapropèle, mer

26   Méditerranée

27

28   Abstract

29   Organic matter degradation is the engine behind the biogeochemical evolution of

30   sediments during burial. Previous research has shown that eogenesis is the seat of a

31   complex interplay between organic matter, microbes and the most reactive part of

32   inorganic compounds, such as clay minerals. To explore the variability and stability of

33   bromine and clay minerals as geochemical and mineral tracers, we selected an

34   eastern Mediterranean core that has a high degree of stability in the quality and

35   quantity of organic matter through time at a one-million-year scale and great

36   variability in organic matter content at a 10 ky scale. According to the very low

37   maximal burial depth reached by these sediments (the core length is only 36.5 m),

38   physical parameters, such as temperature and pressure, did not significantly

39   influence the evolution of the studied parameters during the burial history. The bulk

40   clay mineralogy of organic-rich and organic-poor sediments is similar all along the

41   investigated core material; smectite predominates over kaolinite. The only identified

42   authigenic minerals are biogenetic framboidal pyrite and manganese oxides. The X-

43   ray data and the chemical compositions of the smectite are characteristic of a

44   montmorillonite which is representative of a detrital Nile source. At a one-million-year

45   scale, the organic matter content has no significant influence on clay eogenesis, and

46   detrital smectite and kaolinite remain unchanged. Bromine is present in marine

47   organic matter as organobromine compounds. During eogenesis, bromine is released

48   from organic matter as bromide ion, resulting in an increase in the bromide

49   concentration in the pore water with depth. Dissolved bromide can be used as a

50   conservative tracer of the debromination of sedimentary organic matter. For the first

51   time, we established that solid-phase BrOrg is a reliable tracer of debromination rates

52   in marine sediments. The rate of debromination depends on the organic matter

53   content. The rate increases from less than 2.3×10^{-4} µmolBrOrg molC^{-1} y^{-1} to $6.3 \times$

54   10^{-4} µmolBrOrg molC^{-1} y^{-1} when TOC varies from 0.17 to 3%. This increase is related

55   to the development of the bacterial population and provides the basis for further

56   investigation of other oceanic basins. For TOC values >4%, the rate of debromination

57   decreases. We propose that the bioavailability of organic matter is another factor of

58   variability in the debromination rate.

59   Résumé

60   La dégradation de la matière organique est le moteur de l'évolution biogéochimique

61   des sédiments au cours de l'enfouissement. Les recherches précédentes ont montré

62   que l'éogenèse est le siège d'interférences complexes entre la matière organique,

63   les microorganismes et la partie la plus réactive des composés inorganiques comme

64   les minéraux argileux. Pour étudier la variabilité et la stabilité de traceurs

65   géochimiques et minéralogiques, le brome et les minéraux argileux, nous avons

66   choisi une carotte de Méditerranée orientale qui présente une grande stabilité de la

67   qualité et de la quantité de la matière organique à l'échelle de 1 million d'années et

68   une grande variabilité de cette quantité à une échelle de 10 ka. Considérant le faible

69   enfouissement de ces dépôts (la carotte ne fait que 36,5 m de long), les paramètres

70   physiques comme la température et la pression, n'influencent pas significativement

71   l'évolution des paramètres étudiés. La minéralogie des argiles demeure semblable

72   dans toute la carotte, que les sédiments soient riches ou pauvres en matière

73   organique ; la smectite domine sur la kaolinite. Les seuls minéraux authigéniques

74   identifiés sont la pyrite framboïdale biogénique et des oxydes de manganèse. Les

75 données de diffraction de rayons X et la composition chimique de la smectite

76 correspondent à celles d'une montmorillonite représentative des apports détritiques

77 du Nil. A l'échelle de 1 million d'années, la quantité de matière organique n'influence

78 pas l'éogenèse des minéraux argileux, la kaolinite et la smectite détritique demeurent

79 inchangées. Le brome est dans la matière organique marine sous forme de

80 composés organobromés. Pendant l'éogenèse, le brome est libéré de la matière

81 organique sous forme d'ion bromure, il en résulte une augmentation avec

82 l'enfouissement de la concentration en bromure dans l'eau interstitielle. Le bromure

83 dissous peut être utilisé comme un traceur conservatif de la débromination de la

84 matière organique sédimentaire. Pour la première fois, nous avons établi que le

85 brome organique particulaire est un traceur valide du taux de débromination dans les

86 sédiments marins. Le taux de débromination dépend de la quantité de matière

87 organique. Il augmente de 2.3×10^{-4} µmolBrOrg molC^{-1} y^{-1} à 6.3×10^{-4} µmolBrOrg

88 molC^{-1} y^{-1} quand le Carbone Organique Total (COT) varie de 0.17 à 3%. Cette

89 augmentation est en relation avec le développement des populations bactériennes et

90 fournit une base pour l'étude d'autres bassins océaniques. Pour les teneurs en COT

91 >4%, le taux de débromination diminue. Nous proposons que la biodisponibilité de la

92 matière organique soit un autre facteur de variabilité du taux de débromination.

93 1 Introduction

94 The early evolution of sediments is an important gap in the fundamental

95 understanding of the eogenetic processes during the very shallow burial of both

96 organic and inorganic matter [Barnes et al., 1990; McKinley et al., 2003; Worden and

97 Morad, 2003; Worden and Burley, 2003]. The term eogenesis covers the very

98 shallow diagenesis of both organic and inorganic matter. Eogenetic mineral reactions

99 include the interaction of detrital mineral assemblages with pore water under the

100   influence of a depositional system (Burley, 1993). Such reactions proceed at low

101   temperature and are partly biochemical because they occur most often in the

102   bacterial sulfate reduction zone (Barnes et al., 1990, Surdam et al. 1989).Organic

103   matter degradation is the engine behind the biogeochemical evolution of sediments

104   during burial. Field observations primarily target shallow sediment depths and fast-

105   decaying materials, although organic matter, particularly the most refractory

106   compounds, may degrade on geological timescales [Middelburg, 1989; Arndt et al.,

107   2013]. Previous research showed that eogenesis is the seat of a complex interplay

108   between organic matter, microbes and the most reactive part of the inorganic

109   compounds, such as clay minerals. It has been established that organic matter

110   stabilization occurs through the formation of organo-mineral complexes with layer-

111   silicates, such as expandable clays, which are responsible for the reduction in the

112   bioavailability of organic molecules [Mayer, 1994]. Organic matter and bacteria are

113   known to influence the earliest reaction of non-silicates (sulfides, carbonates) and are

114   suspected to have a role during clay eogenesis [Pryor, 1975; Coleman, 1985;

115   Worden and Morad, 2003]. Moreover, because eogenesis is influenced by the

116   residence time of the pore fluids, the early diagenetic assemblages are also

117   governed by the control of sedimentation, such as climate, the rate of subsidence

118   and the rate of sedimentation [Worden and Burley, 2003].

119   The aim of this study is to highlight both the organic matter and layer silicates

120   evolution during eogenesis based on the variability or stability of bromine and clay

121   mineral geochemical tracers.

122   Inorganic bromine is found as soluble bromine salts in seawater, but there are also

123   numerous (200) known organobromine compounds that are synthesized by living

124   organisms or formed during natural abiotic processes, such as forest fires or volcanic

125   eruption [Gribble, 2003]. Bromine is present in marine organic matter as

126   organobromine compounds, and a direct correlation between the bromine content

127   and organic carbon content of sediments has been found by several authors [Price

128   and Calvert, 1977; Pedersen and Price, 1980; Ten Haven et al., 1988; Martin et al.,

129   1993; Ziegler et al., 2008; Leri et al. 2010]. During eogenesis, bromine is released

130   from organic matter as bromide ion, resulting in an increase in the bromide

131   concentration in pore water with depth [Gieskes and Mahn, 2007]. Dissolved bromide

132   can be used as a conservative tracer of the debromination of sedimentary organic

133   matter [Upstill-Goddard and Elderfield, 1988; Mahn and Gieskes, 2001; Berg and

134   Solomon, 2016]. It is generally accepted that the variations in the source of organic

135   matter, supply rate and initial solid-phase bromine concentration make the solid-

136   phase bromine concentration an unreliable tracer for debromination in marine

137   sediments [Berg and Solomon, 2016]. We assume that it is possible to calculate the

138   debromination rate based on the solid-phase bromine concentration variability

139   through time.

140   To achieve this objective and to explore clay mineral evolution, the studied sediment

141   must satisfy certain requirements. The investigated site must display a high degree of

142   stability through time of: (1) the sediment supply characteristics, (2) the

143   sedimentation rate, which must be moderate to provide limited burial, and (3) the

144   quality and quantity of the organic supply at one-million-year scale. However, to

145   investigate the effect of the total organic carbon (TOC) concentration on

146   debromination and clay mineral evolution, large variability in the organic matter

147   content is required at a 10 ky scale.

148   The sediments of the eastern Mediterranean sea are good candidates to explore the

149   evolution of organic matter during burial and over time. Organic-poor and organic-rich

150 (sapropels) layers occur periodically in the sedimentary sequences due to a recurrent

151 decline in deep-water ventilation. Sapropels have been the subject of many

152 publications since the 1970s; Meyers [2006] and Rohling et al. [2015] are two of the

153 most recent studies. This study focuses on the Neogene sediments of the Nile

154 margin, which are situated in the far eastern Mediterranean sea, a location that

155 enhances the sapropel layer registration in a smectite-rich sedimentary column.

156 2 Material and methods

157 2-1 Material

158 Core MD04 2723 (latitude 32°59.99'N, longitude 33°08.01'E, 1527 m water depth,

159 36.54 m long) was collected on the eastern part of the Nile continental margin during

160 the Vanil cruise of Marion Dufresne II in 2004 (Fig. 1). This margin was built by the

161 Nile river, one of the longest rivers in the world with a summer flood regime. Several

162 high magnitude flood periods occurred during the Quaternary, which have been

163 correlated with the periodic intensification of monsoonal activity over the Nile

164 headwaters [Hassan, 1981; Rossignol-Strick, 1985; Emeis et al., 2000; Kallel et al.,

165 2000; Schilman et al., 2001]. Nile floods and/or enhanced rainfall over the basin

166 represent significant potential sources of fresh water for the Levantine basin. This

167 fresh water increased the density stratification of the water column and organic

168 matter preservation, and nutrients brought in by the runoff enhanced productivity.

169 These conditions can trigger sapropel deposition [Olausson, 1961; Rohling, 1994;

170 Béthoux and Pierre, 1999; Cramp and O'Sullivan, 1999; Jorissen, 1999; Casford et

171 al., 2003; Meyers, 2006; Rohling et al., 2015]. Sapropels are episodic, basin-wide

172 organic-rich layers that characterize the Neogene sedimentary sequences of the

173 Mediterranean Sea. The classic lithostratigraphy of the eastern Mediterranean is

174 based on isochronous sapropel deposits, which are synchronous throughout the

175 deep-water basins [Kroon et al., 1998; Kallel et al., 2000; Ducassou et al., 2007].

176 Sapropels were identified in the studied core based on the lithological characteristics

177 and total organic carbon (TOC) content. They appear as dark greenish and oily

178 layers, laminated or bioturbated depending on their thickness; homogenous, color-

179 banded or composite; with a TOC of at least 1% [Murat and Got, 2000]. The studied

180 core has a continuous and undisturbed sedimentary record of sapropelic sequences

181 numbered from 1 for the youngest to 29 for the oldest according to the usual

182 standard.

183 2-2 Methodology

184 2-2-1 Sampling strategy

185 Core scanner measurements were conducted on a slab collected at the surface of

186 the archive half core. The slabs were then regularly sampled to obtain isotopic data.

187 Geochemical analysis (TOC, Ca and Br) and characterization of clay minerals were

188 performed on samples from the work half core. We considered 18 sapropelic

189 sequences of the available 28 (S1, S3, S5, S6, S7, S9, S10, S11, S12, S15, S17,

190 S19, S21, S23, S24, S27, S28 and S29) to obtain regular information through time

191 and conducted high-frequency sampling. "Sapropelic sequence" refers to a set of

192 samples collected below, inside and above the sapropel itself. Each sapropelic

193 sequence corresponds to a sedimentation period ranging from 10 to 20 ky. We

194 added a series of non-sapropelic samples deposited between 17 and 60 ka during

195 isotopic stages 2 to 4.

196 To match the data obtained from the archive slab and work half core, lithologic

197 description was performed for both. The final lithologic synthesis was based on the

198 archive slab half core depths. The depths of the work half core samples were

199 recalculated when necessary.

200 2-2-2 Isotope analysis

201 Stable isotope measurements were carried out every 10 cm. Samples were dried at

202 40 °C, weighed, washed and sieved with mesh widths of 63 µm and 150 µm. Isotope

203 measurements were made on the planktonic foraminifera *Globigerinoides ruber* var.

204 *alba* (20 specimens per sample), which were hand-picked from the > 150 µm size

205 fraction.

206 The isotopic composition of carbonate was measured according to the method

207 described in detail in Breitenbach and Bernasconi (2011). Briefly, approximately 60-

208 80 µg of crushed, homogenized foraminifera shells were added to 4.5 ml Exetainers,

209 (Labco, High Wycombe, UK) and flushed with pure helium. The samples were

210 reacted with 3-4 drops of 100% phosphoric acid at 70 °C with a Thermo Fisher

211 GasBench device connected to a Thermo Fisher Delta V mass spectrometer. The

212 average long-term reproducibility of the measurements based on replicated

213 standards was ±0.06‰ for $\delta^{18}O$. The instrument was calibrated with the international

214 standards NBS19 ($\delta^{18}O$ = -2.2‰) and NBS18 ($\delta^{18}O$ = -23.01‰). The isotope values

215 are reported in the conventional delta notation with respect to VPDB (Vienna Pee

216 Dee Belemnite).

217 The age model of MD04 2723 was established by correlation of the oxygen isotope

218 record with the Eastern Mediterranean *G. ruber* stack of Wang et al. (2010) using the

219 Software Analyseries (Paillard et al. 1996).

220 2-2-3 Total organic carbon

221 The sediment samples were freeze-dried, crushed and homogenized for geochemical

222 analysis (total organic carbon, Ca and Br contents). For the analysis of total organic

223 carbon, sediment samples were acidified by H_3PO_4 (1 M) to remove carbonates,

224 dried on a hot plate at 40 °C, and measured by combustion in a LECO CS 300

225 carbon sulfur analyzer. Two or three replicates of dried and homogenized sediment

226 (50 mg) were analyzed per sample.

227 2-2-4 Rock-Eval pyrolysis

228 All samples were analyzed with the Rock-Eval thermal analysis technique, using a

229 RE6 Turbo device (Vinci Technologies). Details of the RE6 apparatus are extensively

230 described in Behar et al. [2001]. Analyses were carried out using the operating

231 principles for the analysis of recent marine sediments. [Baudin et al., 2015]. The RE6

232 technique provided measurements from the sequential pyrolysis and oxidation of

233 approximately 40 mg of desalted crushed sample. The pyrolysis gas effluents (mainly

234 hydrocarbons) were detected and quantified by flame ionization detection (FID), and

235 the evolution of CO and CO_2 gas was quantified by infrared detection during the

236 pyrolysis and oxidation stages. The pyrolysis was carried out from 180 °C to 650 °C

237 in an N_2 atmosphere, whereas the oxidation was carried out from 300 °C to 850 °C in

238 a laboratory air atmosphere.

239 The RE6 technique provides information on the quantity, type (sources) and thermal

240 evolution state of sedimentary organic matter.

241 2-2-5 Bromine and calcium analysis on single samples

242 The bromine and calcium contents were analyzed by X-ray fluorescence using an

243 xSORT instrument (Spectro Ametek). The instrument was set up on a stand, and

244 analyses were performed with the manufacturer's Environ-H program. Ground

245   sediment was placed in a 15 mm diameter plastic cup with a 4 µm thick

246   polypropylene window and was manually compacted. For each sample, four

247   replicates were analyzed during 300 s.

248   For Ca, 25 eastern Mediterranean sediment samples analyzed by ICP-AES (Service

249   d'Analyses des Roches et Minéraux, SARM - Nancy). A range of concentrations from

250   3 to 10% was used to calibrate the equipment. The detection limit was 50 ppm, and

251   the replicates agree within 5%.

252   For Br, we used standards prepared from a Mediterranean sediment for calibration.

253   The sediment was sieved with a mesh width of 40 µm and high purity water, freeze-

254   dried, crushed and homogenized. Known quantities of KBr solution were added to

255   the sediment subsamples, and the subsamples were freeze-dried, crushed and

256   homogenized. The detection limit was 5 ppm, and the replicates agreed within 5%.

257   The samples were also analyzed for calcium and total bromine (BrTot). Part of the

258   samples was then rinsed twice with ultrapure water to remove residual salt from

259   marine pore-water evaporation. A second analysis was carried out to analyze solid-

260   phase bromine (BrSol). Previous studies have shown that pure water removes Br

261   only to the extent that would be expected from dried interstitial water [Harvey, 1980;

262   Mayer et al., 1981; Mayer et al., 2007] and that insignificant organic bromine was

263   washed away [Mayer et al., 2007].

264   2-2-6 Bromine and calcium analysis by core scanner

265   High-resolution geochemical elemental composition records were measured directly

266   on the archive slab surface with an Avaatech XRF Core Scanner at the EPOC

267   Laboratory (University of Bordeaux). After cleaning and preparation of the slab

268   surface, three separate runs (10, 30 and 50 kV, with currents of 0.6, 1.5 and 2.0 mA,

269 respectively) were performed every 5 mm down-core with a down-core slit size of 5

270 mm. Sampling time was set to 10 s at 10 kV, 15 s at 30 kV and 20 s at 50 kV. The

271 slab surface was covered with a 4 μm thin SPEXCerti Prep Ultralene1 foil to avoid

272 contamination of the XRF measurement unit and desiccation of the sediment. Raw

273 data spectra were processed by the analysis of the X-ray spectra using the iterative

274 least squares software (WIN AXIL) package from Canberra Eurisys. The elements

275 analyzed include a broad range, from aluminum ^{13}Al through uranium ^{92}U (Richter et

276 al, 2006, Tjallingii, 2007). In this paper, we focused on select elements, such as

277 calcium (Ca) and total bromine (BrTot).

278 To transform core scanner relative data into quantitative results, 56 sediment

279 samples were selected within areas of the core scanner signal stability (at least 2

280 cm). Despite uncertainty linked to the variability of the water content, significant

281 correlations were highlighted between the core scanner data on wet sediment

282 samples and the X-ray fluorescence results on dried sediment samples (BrTot, r =

283 0.95; Ca, r = 0.93).

284 2-2-7 Characterization of clay minerals

285 Sediments were gently crushed, and part of the collected powder (grain size less

286 than 50 μm) was added to deionized water to form mineral suspensions, which were

287 dispersed ultrasonically for 2 minutes. The less than 2 μm fraction size of the

288 sediments was collected by sedimentation, and clay minerals were characterized

289 from the XRD patterns of the oriented preparations acquired in air-dried conditions

290 and after ethylene glycol solvation. XRD analyses were performed using a Bruker$^{®}$

291 D8 XRD diffractometer (CuKα radiation). Diffracted beam CuKα^{1+2} radiation was used

292 (40 kV, 40 mA) and collected by a linxeye detector. Relative humidity was not

293 controlled during data acquisition. The oriented preparation of the less than 2 μm

294   fraction size was analyzed from 2º to 30º 2θ for a detailed characterization of the

295   d00☐ reflections of phyllosilicates.

296   Petrographic studies were performed on the rock fragments using a JEOL 5600 LV

297   SEM equipped with an EDS (BRUKER XFlash 4030 Silicon drift detector). SEM

298   observations were performed in secondary electron imaging mode (SEI) for

299   morphological investigations and backscattering electron mode (BSE) on carbon-

300   coated thin sections for imaging of the chemical contrast and selection of local sites

301   for punctual chemical analysis. The analytical conditions were 15 kV, 1 nA, a

302   counting time of 60 s and a working distance of 16.5 mm. The standards used for

303   EDS consisted of albite (Na, Al, Si), almandine (Mg, Fe), diopside (Ca), orthoclase

304   (K) and spessartite (Mn). Matrix corrections were performed using an integrated

305   program (a PhiRhoz correction). The reproducibility of the standard analyses was

306   nearly 1.5% for all of the elements, except Na, which had a reproducibility of 3%.

307   TEM-EDX microanalyses were conducted on individual particles deposited on a C-

308   coated copper grid using a JEOL JEM 2011 TEM fitted with an X-Flash Silicon Drift

309   Detector 5030 (Bruker). The data collection parameters were set as follows:

310   magnification of 50000 x, 4 L spot size, angular tilt of 20° toward the detector, time

311   constant of 60 $kcp.s^{-1}$, energy range of 40 keV, and corrected counting time of 30 s.

312   The beam diameter was set to ~20 nm to reach the smallest particles.

313   The mid-infrared (MIR) spectra (400 to 4000 cm^{-1}) were acquired on KBr pellets

314   using a Nicolet 760 FTIR spectrometer equipped with a potassium bromide (KBr)

315   beamsplitter and a DTGS-KBr detector. The resolution was set to 4 cm^{-1}, with a co-

316   addition of 100 scans. KBr pellets contained 1 mg of sample for every 150 mg of KBr

317   powder, which was crushed into a mortar and pressed under 8 tons for 5 minutes in a

318   hydraulic press before drying at 120 °C.

319   2-2-8 Quantification of the relative amounts of kaolinite and smectite

320   The relative amounts of kaolinite and smectite (smectite/kaolinite ratio) of the natural

321   samples were obtained from normalized near infrared spectra according to the

322   methodology described by Hébert et al. [2015]. Near-infrared spectra were collected

323   in reflectance mode using a Nicolet 750 FTIR spectrometer with an integration

324   sphere accessory. The spectrometer was equipped with a white light source, a CaF_2

325   beam splitter and a PbSe detector. Spectra over the 10000-4000 cm^{-1} wavenumber

326   range were obtained by co-addition of 100 spectra with 4 cm^{-1} resolution. For

327   measurements, a few hundreds of milligrams of samples were either placed directly

328   onto the integration sphere's shutter or disposed into IR-transparent flasks when

329   unconsolidated.

330   Kaolinite and smectite have several atomic bonds within their crystal structure that

331   absorb radiation in the near-infrared domain. The absorption bands of kaolinite and

332   smectite can be observed in two regions of the infrared spectrum: from 1350 to 1500

333   nm (for overtones of OH stretching vibrations) and from 2100 to 2400 nm (for the

334   combination of OH stretching and bending vibrations). The absorption bands of

335   kaolinite and smectite overlap in the two regions of interest. However, kaolinite has a

336   diagnostic absorption feature at 2165 nm, and the relative proportions of smectite

337   and kaolinite can be determined by deconvolution of the four infrared (IR) bands that

338   are overlapped in the region between 2100 nm and 2300 nm (Hébert et al., 2015).

339   The smectite/smectite+kaolinite ratio calculated using this method corresponds to the

340   percentage of smectite in the clay material, which will be referred to as Sm%

341   hereafter.

342 2-2-9 Statistical analysis

343 Because each variable in the datasets used here can contain error [Laws and Archie,

344 1981; Sokal and Rohlf, 2012], we applied Model II regression to determine the

345 correlations between the studied variables. This model prevents underestimation of

346 the regression slope [Riker, 1973]. Regression analysis was performed using the

347 lmodel2 package from R language (R Development Core Team, 2013). The statistical

348 level of significance was defined at $p<0.05$ (Spearman's rank correlation test).

349 3 Results

350 3-1 Sediment characteristics

351 The stratigraphic framework was established based on the $\delta^{18}O$ isotopic record (Fig.

352 2). The core displays a complete record of the last 1080 ky. According to the very low

353 maximal burial depth reached by these sediments (the core length is only 36.5 m),

354 physical parameters, such as temperature and pressure, did not significantly

355 influence the evolution of the studied parameters during the burial history.

356 Deposits are characterized by cyclic sedimentation of organic-rich sapropel layers

357 and organic-poor hemipelagic to pelagic sediments. Based on the sediment

358 thickness, and without considering the upper sediment column (0-6.5 m), which was

359 stretched by coring, the sedimentation rate varies slightly between 3.5 cm ky^{-1} (6.5-

360 20.0 m) and 2.8 cm ky^{-1} (20.0-36.5 m). The Ca concentration varies from 3.2 to

361 22.4%, which corresponds to a carbonate content of 8 to 56% (Fig. 2). The upper

362 part of the core (0-493 ka) displays slightly higher values, with a mean of 11.9%, than

363 the lower part (493-1084 ka), with a mean of 10.5%. Thus, the Ca content exhibits a

364 weak but significant anticorrelation with age (N=7250, r=-0.23).

365   According to the discrete occurrence of sapropels in the sedimentary column, the

366   organic carbon content has high variability (0.17 to 6.74%, S5 sequence for example)

367   on a small scale (10 to 20 ky) but is stable on a 1 my scale (Fig. 2). Correlation tests

368   prove that the TOC and age are independent variables (N=323, r=-0.08). The

369   quantity of organic matter is constant through time.

370   Rock-Eval pyrolysis was originally developed to characterize the organic matter

371   present in oil source rocks [Espitalié et al., 1977], which are typically more thermally

372   mature and at higher concentrations than thermally immature marine sediments, like

373   the Mediterranean sapropels. Rock-Eval analyses have proved valuable in helping to

374   determine organic matter sources and the state of diagenetic transformation in

375   immature sediment samples [Bouloubassi et al., 1999; Baudin et al., 2007;

376   Tribovillard et al., 2008; Hatcher et al., 2014]. The hydrogen (HI) and oxygen indexes

377   (OI) are related to the atomic composition of the total organic matter and are

378   commonly plotted against each other in a modified van Krevelen-type plot (Fig. 3), in

379   which three main types of organic matter and their thermal alteration routes are

380   defined [Tissot and Welte, 1984].

381   The oxidation of organic matter affects both the HI and OI. As marine organic matter

382   (Type II) is oxidized, there is a shift to lower HI and higher OI, and the HI-OI plot

383   approaches the characteristics of Type III vascular plant organic matter [Bouloubassi

384   et al., 1999 on the eastern Mediterranean ODP site 969]. The results of the Rock-

385   Eval analyses of sapropels from MD04 2723 exhibit a similar trend (Fig. 3). High

386   organic carbon sapropel samples correspond to marine Type II organic matter that is

387   well preserved and lower organic carbon to mainly altered marine organic matter.

388   Microbial alteration of the organic matter during sinking or in the upper sediment

389   layers, particularly by sulfate-reducing bacteria, has been reported to reduce the HI

390   [Vetö et al., 1994]. The significant positive correlation between HI and TOC supports

391   this interpretation (N=20, r=0.89).

392   3-2 Bromine

393   BrTot varies from 32 to 344 ppm, with a mean of 74 ppm (Fig. 2). This variability

394   reflects the variation in the organic matter content; higher BrTot concentrations

395   correspond to sapropel layers. Statistical analysis of the dry sediment samples shows

396   a significant correlation (N=323, r=0.90) between BrTot and TOC. Despite this BrTot-

397   TOC correlation, a slight but significant evolution can be shown with the age

398   (N=7250, r=-0.22). Without the sapropel layers, the anticorrelation is weaker

399   (N=6335, r=-0.17). BrTot decreases through time, while TOC is constant.

400   To further explore this debromination, particular attention is paid to solid-phase

401   bromine (BrSol). BrSol and TOC display a highly significant relationship (N=63,

402   r=0.92) (Fig. 4 and Tab. 1).

403   The intercept of the all data regression lines tend towards zero. This proves that

404   BrSol is bromine linked to organic matter (BrOrg). This direct correlation between the

405   bromine content and the organic carbon content of marine sediments has been

406   demonstrated by several authors [Price et al., 1970; Price and Calvert, 1977;

407   Pedersen and Price, 1980; Martin et al., 1993; Ziegler et al., 2008; Leri et al., 2010].

408   The BrOrg results are in close proximity for low TOC contents and become more

409   scattered with increasing TOC. This dispersion can be explained by the age of the

410   samples. The more recent sapropelic sequences exhibit higher BrOrg than the older

411   ones at equivalent TOC concentrations. The analysis of this issue by sapropelic

412   sequences is presented in Table 1.

413   The correlations are highly significant for the S1, S5, S17 and S28 sequences. The

414   numbers of samples are too low for the S9, S10 and S12 sequences; therefore, the

415   correlations are not statistically valid. Nevertheless, the different sequences display a

416   consistent trend of a decreasing slope with age (Fig. 5).

417   However, it remains to be determined whether the organic carbon content can affect

418   debromination. To highlight this possibility, we selected 4 data sets corresponding to

419   different TOC ranges and examined the evolution of BrOrg through time for each of

420   them (Fig. 6 and Tab. 2). We chose narrow ranges of TOC (0.5 to 0.8%) and, when

421   possible, a broad range of ages.

422   Organic-poor samples (TOC<0.5%) do not show significant evolution through time

423   (N=16, r=-0.17, NS), i.e., our dataset does not allow us to demonstrate a change with

424   age. BrOrg is always low and remains almost constant.

425   In contrast, the 1.5-2.3% and 2.3-3% TOC ranges show significant linear correlations

426   of BrOrg with age, i.e., the higher the TOC range, the steeper slope, and the higher

427   correlation coefficient (Table 2).

428   The rate of debromination (DBrR) increases with TOC content. For a mean TOC of

429   0.24%, BrOrg is almost stable (it varies from <5 to 12 ppm during 1 my). DBrR

430   cannot be calculated, but is low. For a mean TOC of 1.83%, BrOrg decreases from

431   68 to 40 ppm in 1 my, and DBrR = 2.3 x 10^{-4} µmolBrOrg molC^{-1} y^{-1}. For a mean TOC

432   of 2.73%, BrOrg decreases from 147 to 32 ppm in 1 my, and DBrR increases to 6.3 x

433   10^{-4} µmolBrOrg molC^{-1} y^{-1}.

434   For an organic carbon content greater than 4%, the data are scarce. Only five

435   sapropel layers reach this level of TOC, and long periods of time are without data

436   (Fig. 2). Compared to the other ranges studied, the variability of BrOrg is greater for

437 samples of similar TOC and age and outliers appear. The results obtained for the full

438 range (4.0-6.5%) are comparable to those derived from the more limited ranges

439 (4.55-4.95% and 5.4-6.4%). However, the slopes of the calculated regression lines

440 are lower than that for the 2.3-3% TOC range, approximately -0.07. There is an

441 unexpected decrease in the rate of debromination to approximately 2.0×10^{-4}

442 $\mu molBrOrg\ molC^{-1}\ y^{-1}$.

443 The intercepts provide an indication of the initial quantity of BrOrg, i.e., the quantity at

444 the time of deposit, so it is possible to calculate the initial value of BrOrg/TOC (Table

445 2). For the <0.5% range, the initial BrOrg/TOC (weight ratio 29×10^{-4}, molar ratio 4.4

446 $\times 10^{-4}$) is in accordance with the value of the younger sample (weight ratio 30×10^{-4},

447 molar ratio 4.5×10^{-4}, for 2 ka). Likewise, for the 1.5-2.3% range, the initial

448 BrOrg/TOC (weight ratio 37×10^{-4}, molar ratio 5.6×10^{-4}) is in accordance with the

449 value of the younger sapropel (N=4, weight ratio 37.8×10^{-4}, molar ratio 5.7×10^{-4} for

450 8 ka). For the higher TOC ranges, the youngest samples are too old for a valuable

451 comparison. For the 2.3-3.0% range, the initial calculated BrOrg/TOC is increasing

452 (weight ratio 54×10^{-4}, molar ratio 8.1×10^{-4}). However, for higher TOC (4.0-6.5%

453 range) the initial calculated BrOrg/TOC is decreasing (weight ratio 37×10^{-4}, molar

454 ratio 5.6×10^{-4}).

455 The solid-phase organic bromine-age relationship holds in the organic-rich

456 sediments, whereas it fails in the organic-poor sediments

457 3-3 Clay minerals

458 The bulk clay mineralogy of the organic-rich and organic-poor sediments is similar all

459 along the investigated core material. The XRD patterns obtained from the oriented

460 mounts of the less than 2 µm fraction size of the sediments indicate that their clay

461 material is primarily a mixture of smectite and kaolinite, with minor amounts of micas

462 [muscovite] and subordinated chlorite. Similar clay mineralogical composition has

463 been described on the Nile margin [Maldonado and Stanley, 1981; Stanley et al.,

464 1998; Hamann et al., 2009]. Smectite predominates in all samples. It was identified

465 from its broad d_{001} reflection toward 15 Å in the air-dried preparation of Ca-saturated

466 samples that expands to 17 Å and the occurrence of a harmonic d_{002} reflection close

467 to 8.5 Å after saturation with ethylene glycol (Fig. 7).

468 The large width at half maximum height (FWMH > 1.5°2θ) of the d_{001} reflection and

469 the very low intensity of the d_{002} reflection of the smectite after ethylene glycol

470 saturation (which makes it difficult to identify in the XRD pattern) is indicative of the

471 low coherent scattering domain size (CSDS) of smectite crystallites. Kaolinite is

472 characterized by typical d_{001} and d_{002} reflections at 7.16 Å and 3.57 Å, respectively.

473 From a comparative study of the XRD patterns of all samples, it can be observed that

474 the intensity ratio between the d_{001} reflections of smectite and kaolinite significantly

475 varies all along the sapropelic sequence.

476 SEM observations indicate that very fine-grained clay particles (less than 2 μm) are

477 intimately mixed with calcareous micro- to nano-fossil oozes, particles of

478 carbonaceous material and very fine-grained detrital mineral, such as micas, alkali

479 feldspars and quartz. The authigenic minerals identified by petrographic observation

480 consist only of spherical aggregates of octahedral pyrite (framboidal pyrite), which is

481 very common within the organic-rich sediments (Fig. 8), and tiny crystals of

482 manganese oxides that have been observed locally in proximity to the sapropelic

483 horizons.

484 When observed after dispersion in water and sedimentation on a glass substratum

485 (Fig. 8b), the clay particles present a typical morphology of smectite (i.e., resulting in

486 the aggregation of thin films of clay minerals with anhedral morphology) intimately

487 associated with more dispersed subhexagonal plates of kaolinite. HRTEM

488 observation of the smectite tactoids indicates that they are composed of very thin

489 crystallites, which display a very small number of stacked individual layers (less than

490 5) when oriented perpendicularly to c* (Fig. 8c). This is in agreement with the XRD

491 data, which indicated the low coherent scattering domain size (CSDS) of the smectite

492 crystallites.

493 The crystal-chemical characteristics of the smectite particles do not change

494 significantly along the investigated core. Despite a relatively large range of chemical

495 variation, which results from intimate mixing with different types of mineral impurities,

496 the punctual analyses obtained from SEM-EDX and TEM-EDX converge toward a

497 composition of montmorillonite (Table 3).

498 All structural formulas are characteristic of dioctahedral smectite with octahedral

499 occupancy ranging from 2 to 2.1 atoms per formula unit (a.p.f.u.), in which the

500 tetrahedral negative charge (due to substitution of Al with Si) is very low (less than

501 0.2). Despite the uncertainty in the partitioning of Mg between the octahedral sheet

502 and interlayer position and the Fe^{2+}/Fe^{3+} ratio within the octahedral sheet, the

503 negative charge of the 2:1 layer is due to Mg^{2+} for Al substitution. The

504 montmorillonitic composition of the smectite of both organic-rich and organic-poor

505 sediments is confirmed by the middle-infrared spectra of the clay material. The OH

506 bending bands of the phyllosilicates between 820 and 915 cm^{-1} agree with the

507 dioctahedral nature of the clay minerals (kaolinite and smectite) contained in the

508 sample [Farmer, 1974]. Both kaolinite and smectite contributed to the 912 cm^{-1} band,

509 which was attributed to an AlAl-OH vibration. The 875 and 835 cm^{-1} absorption bands

510   were attributed to $AlFe^{3+}$-OH and $AlMg^{2+}$-OH bending vibrations, respectively

511   [Farmer, 1974, Petit and Decarreau, 1990, Petit et al., 2002].

512   The quantitative analysis of the relative amounts of smectite and kaolinite in the bulk

513   samples by NIR spectrometry (Figure 9) confirms that smectite largely predominates

514   over kaolinite all along the investigated core.

515   The range of variation of the percentage of smectite in the clay material (Sm%) is

516   restricted between 62 and 97% (Fig. 2), and no clear variation can be observed in a

517   comparison of the S/K ratios in the different compartments of the studied core. The

518   range of variation of the Sm% determined at the scale of the sapropelic sequence is

519   often not far from that measured at the core-scale. The smectite content variability

520   cannot be linked to organic matter content variation, and TOC and Sm% are two

521   relatively independent parameters (N=191, r=-0.22, highly significant). The most

522   significant variation of Sm% observed at the core scale is an increase in the smectite-

523   rich samples (Sm%>90) from the bottom (oldest sediments) to the top (younger

524   sediments) of the investigated core.

525   4 Discussion

526   4-1 Debromination

527   There are many ways to explore debromination.

528   One way is BrTot high-frequency core scanner analysis (Fig. 2). Total bromine

529   consists of dissolved bromine and solid-phase bromine. The solid-phase bromine is

530   linked to organic matter and immobilized, but it progressively leaves the organic

531   matter and is released as bromide into pore water. Therefore, it decreases with age.

532   The dissolved bromine is composed of two components: (1) bromide provided by

533   marine pore-water salt at the time of deposition and debromination and (2) organic

22

534 bromine. No significant chemical uptake processes are known to act as a sink for

535 bromide [Berg and Solomon, 2016]. Without the influence of other processes, BrTot

536 will remain constant. However, dissolved bromine is mobile. When debromation

537 occurs, the bromide concentration increases in the pore water more strongly in the

538 organic-rich layers than in the organic-poor layers. As a result, bromide is firstly

539 transported by diffusion from organic-rich to organic-poor sediment to equalize the

540 concentrations. On a larger timescale, bromide migrates through diffusion and/or

541 advection back toward the overlying ocean. The end result is that BrTot and its

542 variability range decrease with age, even though the bromide/chloride ratio increases

543 with depth [Berg and Solomon, 2016]. The MD04 2723 core scanner data exhibits

544 this general trend, whereas TOC remains constant at the same timescale, which

545 supports the debromation of the organic matter and the upward bromide migration.

546 However, BrTot and bromide/chloride ratio analysis provide a limited estimation of

547 debromation itself. Another way to obtain more accurate values is to compare BrTot

548 and the organic carbon content of organic-rich sediment layers. When TOC is high,

549 BrTot is mainly composed of bromine linked to organic matter and the pore-water

550 bromide can be neglected. The core MD04 2723 contains two highly organic-rich

551 sapropel layers: S5 and S28 (Fig. 2). They have similar maximum TOC contents

552 (6.7% for S5 and 6.4% for S28) and different BrTot maximum concentrations (326

553 ppm for S5 and 174 ppm for S28). The debromation rate can be estimated at 3.5 x

554 10^{-4} µmolBrOrg $molC^{-1}$ y^{-1}, in accordance with results obtained directly by the BrOrg

555 measurements (Tab. 2).

556 Studying BrOrg variability is a better way to obtain accurate values of the

557 debromation rates. There are two pathways acting simultaneously in biological

558 systems for the production of BrOrg, biotic production in cells of macro and

23

559 microalgae as a result of the enzymatically mediated reaction of Br^- and abiotic

560 production by nucleophilic substitution [Ballschmiter, 2003]. These reactions produce

561 aliphatic and aromatic forms of organobromine [Leri et al., 2014]. During organic

562 matter degradation, bromine can be removed from organobromine compounds

563 through microbial metabolic or abiotic debromination processes. One metabolic

564 pathway in the degradation of organic material is organohalide respiration. Bacteria

565 in anoxic environments utilize reductive dehalogenase to break the carbon-halogen

566 bond of organohalide compounds functioning as electron acceptors. The bromine is

567 replaced by a hydrogen atom. It has been hypothesized that this metabolic pathway

568 using reductive dehalogenase may be an important energy source for microbial

569 communities in the deep biosphere [Futagami et al., 2009]. The energy yield of

570 organohalide respiration in the natural environment can be several times greater, on

571 a per mole basis, than other metabolic pathways, such as sulfate reduction and

572 methanogenesis [Dolfing, 2003]. Bacterial groups that have the potential to use

573 organohalide respiration as a metabolic pathway have been found to be abundant in

574 deep subsurface marine sediments, both geographically and with depth [Futagami et

575 al., 2009; Orcutt et al., 2011]. Less is known about organohalide fermentation, but it

576 has been shown to be another potential energy-producing pathway for microbes in

577 the deep biosphere [Justicia-Leon et al., 2012; Lee et al., 2012]. Based on the BrOrg

578 concentration variability, we have demonstrated that the rates of debromination are

579 linked to the TOC contents. They increase from less than 2.3×10^{-4} µmolBrOrg molC^{-1}

580 y^{-1} up to 6.3×10^{-4} µmolBrOrg molC^{-1} y^{-1} when TOC varies from 0.17 to 3%. For

581 higher TOC values, precise rates of debromination could not be reliably established

582 due to scattered data (Fig. 6), but they decrease in all cases. To explore the

583 relationship between TOC and the rate of debromination, two assumptions are

584   proposed: the rate of debromination depends on microbial activity and/or the

585   bioavailability of organic matter. Cragg et al. (1998) studied the bacterial

586   concentrations at the eastern Mediterranean ODP site 969, which has similar cyclic

587   sedimentation of organic-poor and organic-rich (80 sapropels beds to 116 mbsf)

588   sediments. Within the range of TOC concentrations usually encountered in marine

589   sediments (0-3%), the data set produced a significant correlation between TOC and

590   bacterial populations, in good agreement with the general profile derived from other

591   ODP sites. The addition of data with higher TOC destroyed the relationship, which

592   suggests that at high concentrations, such as those found in sapropels, TOC is

593   effectively present in excess and ceases to be a limiting factor for bacterial population

594   size. The remarkable fact that the bacterial populations and rates of debromination

595   both increase with the TOC concentration but only within the 0-3% range suggests

596   that debromination is quantitatively dependent on microbial activity. However, it is

597   difficult to explain why the TOC concentration does not behave as a limiting factor

598   when its content is greater than 3%. Cragg et al. (1998) suggested that organic

599   carbon within the sapropel layers must be predominantly recalcitrant and only slowly

600   bioavailable.

601   The organic carbon content of the sapropel layers depends on the rate of

602   degradation/preservation of organic matter. During sapropelic periods, the water

603   column is stratified. The upper layer is normally oxygenated, and aerobic organic

604   matter degradation by microorganisms occurs. The lower layer is oxygen-depleted,

605   and organic matter is oxidized through various less-effective anaerobic pathways

606   [Demaison and Moore, 1980; Emerson and Hedges, 1988]. We assume that very

607   stable stratification results in a high-TOC sapropel (more than 3%), and low organic

608   carbon sapropels correspond to instable stratification with periodic reoxygenation of

25

609   the entire water column [Casford et al., 2003; Stefanelli et al., 2005 and Meyers et al.,

610   2006; Rohling et al., 2015]. The two degradation pathways produce different organic

611   molecules, which are less bioavailable in the case of oxygen-depleted conditions.

612   Therefore, in organic carbon-rich sapropels (TOC > 3%) organic matter would not be

613   as bioavailable as in low organic carbon sapropels (TOC < 3%). Furthermore, the

614   initial BrOrg/TOC also decreases at the 3% TOC. The sediments with 2.3-3.0% TOC

615   provide ideal conditions for the development of bacterial groups that may have the

616   potential to use organohalide respiration: a high content in Br-rich organic matter.

617   Sediment with higher TOC has higher BrOrg content but a lower initial BrOrg/TOC

618   and could be less attractive.

619   However, some factors of the debromination rate variability for very high organic

620   carbon content remain to be identified. We need to explain why two samples

621   collected 3 cm apart within the same sapropel (S17) with the same TOC

622   concentration (4.7 and 4.8%) present different BrOrg contents (140 and 86 ppm). The

623   first cited sample follows the general debromination trend, whereas the second

624   displays evidence of a higher rate (Fig. 6). Therefore, sometimes high rates of

625   debromination occur, even for high organic carbon content layers. The explanation of

626   this difference does not lie in the burial conditions, which are the same. Rather, the

627   solution is in the initial organic matter quality, which is dependent on the production

628   and/or degradation conditions. A 1 cm thick sample corresponds to three centuries of

629   basin history, a duration cannot analyze the climatic variability of the temperature

630   sea-surface, Nile floods or depth of the oxic/anoxic water interface, three parameters

631   that may have influenced the quality of the produced and preserved organic matter

632   [Meyers, 2006]. Sapropels are organic-rich layers, but for most of them, preserved

633   organic matter represents a small portion of the produced organic matter. For low

634 TOC content sapropels (1-3%), the initially produced marine organic matter is mainly

635 degraded. Thus, the degradation step plays a major role in the quality of the finally

636 preserved organic matter. In contrast, for higher organic carbon sapropels, even if the

637 degradation pathways remain important, a higher proportion of produced organic

638 matter is preserved and the quality of the produced organic matter is a more

639 important factor in the variability of bioavailability.

640 4-2 Clay mineral evolution

641 The core MD04 2723 provides an opportunity to examine the evolution of layer

642 silicates in parallel to that of organic matter during the last million years of

643 sedimentation and eogenesis of sediments in the eastern part of the Egyptian

644 continental margin. Kaolinite and smectite are known to be the diagnostic clay

645 minerals of the eogenesis of mudstones (Burley, 1993 and references therein).

646 However, it is unclear whether these clay minerals originate from sedimentation

647 (detrital clays) and/or from the eogenesis of the sediments during their incipient

648 burial.

649 This study shows that (1) there is no evidence of authigenic clay minerals and that (2)

650 dioctahedral smectite largely predominates over kaolinite in the samples collected all

651 along the core MD04 2723. More specifically, infrared spectroscopy and

652 microchemical analyses indicated that the crystal chemistry of the dioctahedral

653 smectite agrees with that of montmorillonite. Its mineralogical and chemical

654 composition is similar to that of the smectite previously identified in the Nile

655 suspended matter [Dekov et al., 1997] and the Nile alluvial soils in Egypt [Kishk et al.,

656 1976] and the range of Sm% measured all along the core is in full agreement with the

657 published clay mineral data from the Nile assemblage [Hamann et al., 2009]. On the

658 basis of the qualitative analysis in this study, it is assumed that the clay mineralogy of

659   the core MD04 2723 is essentially representative of the detrital Nile source. However,

660   on the basis of quantitative analysis, Sm% variability is likely to occur at two different

661   timescales.

662   Some sapropelic sequences exhibit a wide range of variation in Sm% (S10, for

663   example, 71-97%, Fig. 2) while others do not (S15, for example, 66-73%, Fig. 2). The

664   highest Sm% can be located either in the organic-rich (S10 and S11 sequences) or in

665   the organic-poor (S7 and S9 sequences) sequences. The controlling factor of the

666   Sm% variation is not climatic because all four aforementioned sapropels correspond

667   to low values of the $\delta^{18}O$ isotopic record. As expected from the absence of diagenetic

668   evolution of clay minerals, the smectite concentration and TOC are not correlated.

669   Over a span of one million years, a slight change occurs, which is highlighted by the

670   mean values for each sapropelic sequence (Fig. 10).

671   The lower part of the core (500 to 1080 ka) is characterized by a nearly constant and

672   low (69-73%) Sm%, whereas the upper part is characterized by heterogeneous mean

673   values with successively increasing or decreasing gradients (Sm% between 71 and

674   88%), which cannot be linked to the $\delta^{18}O$ isotopic record. The 500 ka limit also

675   affects others sedimentary parameters, such as the Ca concentration and

676   sedimentation rate. The last 500 ky shows an increase in the sedimentation rate, the

677   carbonate content and the Sm% variability. Even though the cause of these

678   variations remains uncertain, the hypothesis of temporal change in detrital sources

679   can be invoked.

680   5 Conclusion

681   The studied site displays both a high degree of stability in the organic supply at a

682   one-million-year scale and great variability in the organic matter preservation at a 10

683   ky scale, an ideal situation to highlight and discuss the influence of the organic matter

684   content on the mineralogical and geochemical evolution during eogenesis. This

685   allows us to demonstrate that at a one-million-year scale, the organic matter content

686   has no significant influence on clay eogenesis. Detrital smectite and kaolinite remain

687   unchanged everywhere, even within the sapropels where high bacterial populations

688   are active.

689   We have demonstrated that solid-phase BrOrg is a reliable tracer of debromination

690   rates in marine sediments. Based on the highly variable TOC concentration of the

691   eastern Mediterranean sea, it was determined that the rates of debromination

692   depend on the organic matter content. This observation provides the basis for further

693   investigation of other oceanic basins. Within the range of TOC concentrations usually

694   encountered in marine sediments (0-3%), both bacterial populations and the rates of

695   debromination increase with TOC content. It can be assumed that these two

696   parameters are correlated. The increase in bioavailable organic matter induces

697   growth of active bacterial populations, resulting in higher rates of debromination. In

698   the eastern Mediterranean sea, the depth profile of the bacterial populations is in

699   good agreement with the general profile derived from other oceans [Cragg et al.,

700   1998; Parkes et al., 2014]. This suggests that the rates of debromination obtained in

701   the Mediterranean sea are relevant for all ocean basins. This assumption should be

702   supported by further investigations, which could be performed on a basin that

703   displays a high and stable organic carbon content over time. This approach would

704   provide only one rate of debromination. It would be more interesting to search for a

705   Mediterranean-like basin that exhibits both a high degree of stability of the organic

706   supply at a one-million-year scale and great variability in the organic matter content

707   at a 10 ky scale. Different rates of debromination could be investigated. Extending

708 the time-range of the sedimentation and diagenetic evolution to a ten-million-year

709 scale would show whether clay minerals remain stable over a one-million-year scale

710 due to of slow reaction kinetics.

711

712 Acknowledgements

717

718 References:

719 ARNDT S., JØRGENSEN B.B., LAROWE D.E., MIDDELBURG J.J., PANCOST R.D.

720 & REGNIER P. (2013). - Quantifying the degradation of organic matter in marine

721 sediments: A review and synthesis. - *Earth-Science Reviews*, **123**, 53–86

722 BALLSCHMITER K. (2003). - Pattern and sources of naturally produced

723 organohalogens in the environment: biogenic formation of organohalogens. -

724 *Chemosphere*, **52**, 313–324.

725 BARNES M. A., BARNES W.C. & BUSTIN R. M. (1990). - Chemistry and diagenesis

726 of organic matter in sediments and fossil fuels. *In:* Geoscience Canada Reprint

727 Series, Diagenesis, 189-204.

728 BAUDIN F., COMBOURIEU-NEBOUT N. & ZAHN R. (2007). - Signatures of rapid

729 climatic changes in organic matter records in the western Mediterranean Sea during

730 the last glacial period. – *Bull. Soc. Géol. Fr.*, **178**, 1, 3-13.

731   BAUDIN F., DISNAR J.P., ABOUSSOU A. & SAVIGNAC F. (2015). - Guidelines for

732   Rock–Eval analysis of recent marine sediments. – *Org. Geochem.*, **86**, 71–80.

733   BEHAR F., BEAUMONT V. & DE PENTEADO, H.L. (2001). - Rock–Eval 6

734   technology: performances and developments. - *Oil and Gas Science and*

735   *Technology,* **56**, 111–134.

736   BERG R.D. & SOLOMON E.A. (2016). - Geochemical constraints on the distribution

737   and rates of debromination in the deep subseafloor biosphere. – *Geochim.*

738   *Cosmochim. Acta*, **174**, 30–41.

739   BÉTHOUX J.P. & PIERRE C., (1999). - Mediterranean functioning and sapropel

740   formation: respective influences of climate and hydrological changes in the Atlantic

741   and the Mediterranean. - *Mar. Geol.,* **153**, 29–39.

742   BOULOUBASSI I., RULLKÖTTER J. & MEYERS, P.A. (1999). - Origin and

743   transformation of organic matter in Pliocene–Pleistocene Mediterranean sapropels:

744   organic geochemical evidence reviewed. - *Mar. Geol.,* **153**, 177–197.

745   BREITENBACH S.F.M. & BERNASCONI S.M. (2011). - Carbon and oxygen isotope

746   analysis of small carbonate samples (20 to 100 µg) with a GasBench II preparation

747   device. - *Rapid Communications in Mass Spectrometry,* **25**, 1910-1914.

748   BURLEY S. D. (1993). - Models of burial diagenesis for deep exploration plays in

749   jurassic fault traps of the central and Northern North Sea. - *Geological Society,*

750   *London, Petroleum Geology Conference series 1993*, **4**, 1353-1375.

751   CASFORD J.S.L., ROHLING E.J., ABU-ZIED R.H., JORISSEN F.J., LENG M. &

752   THOMSON J. (2003). A dynamic concept for eastern Mediterranean circulation and

753   oxygenation during sapropel formation. - *Palaeogeogr. Palaeoclimatol. Palaeoecol.*,

754   **190**, 103–119.

755   COLEMAN M. L. (1985). - Geochemistry of non silicate minerals: kinetic

756   considerations. - *Philosophical Transaction of the Royal Society of London*, **315**, 39-

757   56.

758   CRAGG B. A., LAW K.M., CRAMP A, & PARKES R.J. (1998). - The response of

759   bacterial populations to sapropels in deep sediments of the Eastern Mediterranean

760   (site 969). – *In:* A.H.F Robertson, K.-C. Emeis, C. Richter, & A. Camerlenghi Eds.,

761   Proceedings of the Ocean Drilling Program, Scientific Results, Vol. 160, Texas A&M

762   University, College Station, TX, 303-307.

763   CRAMP A. & O'SULLIVAN G. (1999). - Neogene sapropels in the Mediterranean: a

764   review. - *Mar. Geol.,* **153**, 11–28.

765   DEKOV V.M., KOMY Z., ARAUJO F., VAN PUT A. & VAN GRIEKEN R. (1997). –

766   Chemical composition of sediments, suspended matter, river water and ground water

767   of the Nile (Aswan-Sohag traverse). – *The science of the total environment*, **201**,

768   195-210.

769   DEMAISON G.J. & MOORE G.T. (1980). - Anoxic environments and oil bed genesis.

770   -*Am. Assoc. Pet. Geol. Bull.*, **64**, 1179–1209.

771   DOLFING J. (2003). - Thermodynamic Considerations for Dehalogenation. – *In*: M.

772   M. Häggblom, I. D. Bossert Eds, Dehalogenation: Microbial Processes and

773   Environmental Applications. Springer, 89–114.

774   DUCASSOU E., CAPOTONDI L., MURAT A., BERNASCONI S., MULDER T.,

775   GONTHIER E., MIGEON S., DUPRAT J., GIRAUDEAU J. & MASCLE J. (2007). -

776 Multiproxy late quaternary stratigraphy of the Nile deep-sea turbidite system —

777 Towards a chronology of deep-sea terrigeneous systems. – *Sedimentary Geology,*

778 **200**, 1–13.

779 EMEIS K.C., SAKAMOTO T., WEHAUSEN R. & BRUMSACK H.J. (2000). - The

780 sapropel record of the eastern Mediterranean Sea — results of Ocean Drilling

781 Program Leg 160. - *Palaeogeogr. Palaeoclimatol. Palaeoecol.* **158**, 371–395.

782 EMERSON S. & HEDGES J.I. (1988). - Processes controlling the organic carbon

783 content of open ocean sediments. *Paleoceanography,* **3**, 621–634.

784 ESPITALIE J., LAPORTE J.L., MADEC M., MARQUIS F., LEPLAT P., PAULET J. &

785 BOUTEFEU A. (1977). - Méthode rapide de caractérisation des roches mères, de

786 leur potentiel pétrolier et de leur degré d'évolution. - *Rev. Inst. Fr. Pét.*, **32**, 23–42.

787 FARMER V.C. (1974). - The Infrared Spectra of Minerals. - *Monograph, 4. The*

788 *Mineralogical Society*, London, 539 p.

789 FUTAGAMI T., MORONO Y., TERADA T., KAKSONEN A. H. & INAGAKI F. (2009). -

790 Dehalogenation activities and distribution of reductive dehalogenase homologous

791 genes in marine subsurface sediments. - *Appl. Environ. Microbiol.*, **75**, 6905–6909.

792 GIESKES J.M. & MAHN C. (2007). - Halide systematics in interstitial waters of ocean

793 drilling sediment cores. - *Applied Geochemistry*, **22**, 515–533.

794 GRIBBLE G.W. (2003). - The diversity of naturally produced organohalogens.

795 *Chemosphere*, **52**, 289–297.

796 HAMANN, Y., EHRMANN, W., SCHMIEDL, G., & KUHNT, T. (2009). - Modern and

797 late Quaternary clay mineral distribution in the area of the SE Mediterranean Sea. -

798 *Quaternary Research*, **71**, 453-464.

799 HATCHER, P., RAVIN, A., BEHAR, F., BAUDIN, F. (2014). - Diagenesis of organic

800 matter in a 400 m organic rich sediment core from offshore Namibia using solid state

801 13C NMR and FTIR. – *Org. Geochem.*, **75**, 8-23.

802 HARVEY G.R. (1980). - A study of the chemistry of iodine and bromine in

803 marine sediments. - *Mar. Chem.,* **8**, 327–332.

804 HASSAN F.A. (1981). - Historical Nile floods and their implications for climatic

805 change. – *Science*, **212,** 5, 1142–1144.

806 HATCHER P., RAVIN A., BEHAR F. & BAUDIN F. (2014). - Diagenesis of organic

807 matter in a 400 m organic rich sediment core from offshore Namibia using solid state

808 13C NMR and FTIR. – *Org. Geochem.*, **75**, 8-23.

809 HÉBERT B., BEAUFORT D., ROY R., POURADIER A. & JIKIBAYEV R. (2015) -

810 New methods to quantify clay minerals in the uranium deposits hosted in sands of the

811 Chu Sarysu Basin (South Kazakhstan) based on visible and near-infrared field

812 spectrometry. *In: Proc. 13th Biennial SGA Meeting.* - Nancy, France, 587-589.

813 JORISSEN F.J. (1999). - Benthic foraminiferal successions across Late Quaternary

814 Mediterraenan sapropels. - *Mar. Geol.*, **153**, 91–101.

815 JUSTICIA-LEON S. D., RITALAHTI K. M., MACK E. E. & LÖFFLER F. E. (2012). -

816 Dichloromethane fermentation by a Dehalobacter sp. in an enrichment culture

817 derived from Pristine river sediment. - *Appl. Environ. Microbiol.*, **78**, 1288–1291.

818 KALLEL N., DUPLESSY J.-C., LABEYRIE L., FONTUGNE M., PATERNE M. &

819 MONTACER, M. (2000). - Mediterranean pluvial periods and sapropel formation over

820 the last 200 000 years. - *Palaeogeogr. Palaeoclimatol. Palaeoecol.*, **157**, 45–58.

821 KISHK F.M., EL-ATTAR H.A., HASSAN M.N. & EL-SHEEMY H. (1976). -

822 Mineralogical and chemical composition of the clay fraction of some Nile alluvial soils

823 in Egypt. – *Chem. Geol.*, **17**, 295-305.

824 KROON D., ALEXANDER I., LITTLE, M., LOURENS L.J., MATTHEWSON A.,

825 ROBERSTON A.H.F. & SAKAMOTO T. (1998). - Oxygen isotope and sapropel

826 stratigraphy in the eastern Mediterranean during the last 3.2 million years. – *In:*

827 Proceedings of the Ocean Drilling Program, Scientific Results, Leg 160, 181–189.

828 LAWS E.A. & ARCHIE J.W. (1981). – Appropriate use of regression analysis in

829 marine biology. - *Mar.Biol.,* **65**,13–16.

830 LEE M., LOW A., ZEMB O., KOENIG J., MICHAELSEN A. & MANEFIELD M. (2012).

831 - Complete chloroform dechlorination by organochlorine respiration and fermentation.

832 - *Environ. Microbiol.*, **14**, 883–894.

833 LERI A. C., HAKALA J. A., MARCUS M. A., LANZIROTTI A., REDDY C.M. &

834 MYNENI S. C. B. (2010). - Natural organobromine in marine sediments: new

835 evidence of biogeochemical Br cycling. - *Global Biogeochem. Cycles*, **24**, GB4017.

836 LERI A.C., MAYER L.M., THORNTON K.R. & RAVEL B. (2014). - Bromination of

837 marine particulate organic matter through oxidative mechanisms. – *Geochim.*

838 *Cosmochim. Acta*, **142**, 53–63.

839 MC KINLEY J.M., WORDEN R.H. & RUFFELL A.H. (2003). Smectites in

840 Sandstones: a review of the controls on occurrence and behaviour during diagenesis.

841 *In:* R.H. Worden & S. Morad (Eds.), Clay mineral cements in Sandstones. Blackwell

842 Publishing, 109-128.

843 MAHN, C. L. & J. M. GIESKES (2001). - Halide systematics in comparison

844   with nutrient distributions in sites 1033B and 1034B, Saanich Inlet: ODP

845   Leg 169S. - *Mar. Geol.*, **174**, 1‑4, 323‑339.

846   MALDONADO A. & STANLEY D. J. (1981). - Clay mineral distribution patterns as

847   influenced by depositional processes in Southeastern Levantine Sea. -

848   *Sedimentology*, **28**, 21-32.

849   MARTIN J. B., GIESKES J. M., TORRES M. & KASTNER M. (1993). - Bromine and

850   iodine in Peru margin sediments and pore fluids: implications for fluid origins.

851   *Geochim. Cosmochim. Acta*, **57**, 4377–4389.

852   MAYER L.M., MACKO S.A., MOOK W.H. & MURRAY S.M. (1981). – The distribution

853   of bromine in coastal sediments and its use as a source indicator for organic matter. -

854   *Org. Geochem.,* **3**, 37–42.

855   MAYER L.M. (1994). - Surface area control of organic carbon accumulation in

856   continental shelf sediments. - *Geochim. Cosmochim. Acta*, **58**, 1271–1284.

857   MAYER L.M., SCHICK L.L., ALLISON M., RUTTENBERG K. & BENTLEY S. (2007).

858   - Marine vs. terrigenous organic matter in Louisiana coastal sediments: the uses of

859   Bromine: organic carbon ratios. - *Mar. Chem.*, **107**, 244–254.

860   MEYERS P.A. (2006). - Paleoceanographic and paleoclimatic similarities between

861   Mediterranean sapropels and Cretaceous black shales. - *Palaeogeogr.*

862   *Palaeoclimatol. Palaeoecol.,* **235**, 305–320.

863   MIDDELBURG J.J. (1989). - A simple rate model for organic-matter decomposition in

864   marine-sediments. - *Geochim. Cosmochim. Acta*, **53**, 1577–1581.

865 MURAT A. & GOT H. (2000). - Organic carbon variations of the eastern

866 Mediterranean Holocene sapropel: a key for understanding formation processes. -

867 *Palaeogeogr. Palaeoclimatol. Palaeoecol.*, **158**, 241–257.

868 OLAUSSON E. (1961). - Studies of deep-sea cores. - *Reports of the Swedish Deep*

869 *Sea Expedition 1947–1948*, **8**, 353–391.

870 ORCUTT B. N., SYLVAN J. B., KNAB N. J. & EDWARDS K. J. (2011). - Microbial

871 ecology of the dark ocean above, at, and below the seafloor. - *Microbiol. Mol. Biol.*

872 *Rev.*, **75**, 361–422.

873 PAILLARD D., LABEYRIE L. & YIOU P. (1996). - Macintosh Program performs time-

874 series analysis. – *Eos,* Trans. Am. Geophys.Union, **77**, 39, 379–379.

875 PARKES R.J., CRAGG B., ROUSSEL E., WEBSTER G., WEIGHTMAN A. & SASS

876 H. (2014). – A review of prokaryotic populations and processes in sub-seafloor

877 sediments, including biosphere: geosphere interactions. - *Mar. Geol.*, **352**, 409-425.

878 PEDERSEN T. & PRICE N. (1980). - The geochemistry of iodine and bromine in

879 sediments of the Panama Basin. - *J. Mar. Res.,* **38**, 397–411.

880 PETIT S., CAILLAUD J., RIGHI, D. & MADEJOVÁ J. (2002). - Characterization and

881 crystal chemistry of an Fer-rich montmorillonite from Ölberg, Germany. - *Clay*

882 *Minerals,* **37**, 2, 283-297.

883 PETIT S. & DECARREAU A. (1990). - Hydrothermal (200 degrees C) synthesis and

884 crystal chemistry of iron-rich kaolinites. - *Clay Minerals*, **25**, 2, 141-160.

885 PRICE N. B., CALVERT S. E. & JONES P. G. W. (1970). - The distribution of iodine

886 and bromine in the sediments of the South Western Barents Sea. - *Mar. Res.,* **28,** 22-

887 34.

888   PRICE N. B. & CALVERT S. (1977). - The contrasting geochemical behaviours of

889   iodine and bromine in recent sediments from the Namibian shelf. - *Geochim.*

890   *Cosmochim. Acta*, **41**, 1769-1775.

891   PRYOR W. A. (1975). - Biogenic sedimentation and alternation of argillaceous

892   sediments in shallow marine environments. - *Geological Society of America Bulletin*,

893   **86**, 1244-1254.

894   R DEVELOPMENT CORE TEAM. (2013). - R: a Language and Environment for

895   Statistical Computing. 3-900051-07-0 *R Foundation for Statistical Computing*,

896   Vienna, Austria, URL ⟨http://www.R-project.org/⟩.

897   RICHTER T.O., VAN DER GAAST S., KOSTER B., VAARS A., GIELES R., DE

898   STIGTER H.C., DE HAAS H. & VAN WEERING T.C.E. (2006). - The Avaatech XRF

899   Core Scanner: technical description and applications to NE Atlantic sediments. -

900   *Geological Society London, Special Publication*, **267**, 39-50.

901   RICKER W.E. (1973). – Linear regressions in fishery research. - *J. De. l'Off. Des.*

902   *Rech. sur Les. Pêcheries Du. Can.,* **30**, 3,409–434.

903   ROHLING E.J. (1994). - Review and new aspects concerning the formation of

904   Mediterranean sapropels. - *Mar. Geol.,* **122**, 1–28.

905   ROHLING E.J., MARINOA G. & GRANT K.M. (2015). - Mediterranean climate and

906   oceanography, and the periodic development of anoxic events (sapropels). - *Earth-*

907   *Science Reviews*, **143**, 62–97.

908   ROSSIGNOL-STRICK M. (1985). - Mediterranean Quaternary sapropels, an

909   immediate response of the African monsoon to variations of insolation. -

910   *Palaeogeogr. Palaeoclimatol. Palaeoecol.*, **49**, 237–263.

911   SCHILMAN B., ALMOGI-LABIN A., BAR-MATTHEWS M., LABEYRIE, L., PETERNE

912   M. & LUZ, B. (2001). - Long- and short-term carbon fluctuations in the eastern

913   Mediterranean during the late Holocene. – *Geology*, **29**, 12, 1099–1102.

914   SOKAL R.R. & ROHLF F.J. (2012). - Biometry: The Principles and Practice of

915   Statistics. – *in:* W. H. Freeman and Co Eds, Biological Research*, 4th edition., New

916   York*, 937p.

917   STANLEY, D. J., NIR, Y., & GALILI, E. (1998). - Clay mineral distributions to interpret

918   Nile cell provenance and dispersal: III. Offshore margin between Nile delta and

919   northern Israel. - *Journal of coastal Research*, **14**, 196-217.

920   STEFANELLI S., CAPOTONDI L. & CIARANFI N. (2005). – Foraminiferal record and

921   environmental changes during the deposition of the Early-Middle Pleistocene

922   sapropels in southern Italy. – *Palaeogeogr. Palaeoclimatol. Palaeoecol.*, **216**, 27-52.

923   SURDAM R. C., DUNN T. L., HEATHER H.P. & MACGOWAN, D.B. (1989). -

924   Integrated diagenetic modelling; a process orientated approach for clastic systems.

925   *Annual Reviews of Earth and Planetary Science Letters*, **15**, 141-170.

926   TENHAVEN H. L., DELEEUW J. W., SCHENCK P. A. & KLAVER G. T. (1988). -

927   Geochemistry of Mediterranean sediments—Bromine/organic carbon and

928   uranium/organic carbon ratios as indicators for different sources of input

929   and post-depositional oxidation, respectively. - *Org. Geochem.*, **13**, 1–3,

930   255–261.

931 TJALLINGII R., RÖHL U., KÖLLING M. & BICKERT T. (2007). - Influence of the

932 water content on X-ray fluorescence core-scanning measurements in soft marine

933 sediments. - *Geochem. Geophys. Geosyst.*, **8**, Q02004.

934 TISSOT B.P. & WELTE D.H. (1984). - Petroleum Formation and Occurrence. -

935 2nd. ed. Springer, Heidelberg, 601 p.

936 TRIBOVILLARD N., BOUT-ROUMAZEILLES V., SIONNEAU T., MONTERO-

937 SERRANO J.C., RIBOULLEAU A. & BAUDIN F. (2009). - Organic-matter

938 preservation and accumulation in an anoxic setting: the Orca Basin, Gulf of Mexico.

939 *Comptes Rendus Geosciences*, **341**, 1-9.

940 UPSTILL-GODDARD R. C. & ELDERFIELD H. (1988). - The role of diagenesis in the

941 estuarine budgets of iodine and bromine. - *Cont. Shelf Res.,* **8**, 405–430.

942 VETÖ I., HETÉNYI M., DEMÉNY A. & HERTELENDI E. (1994). - Hydrogen index as

943 reflecting intensity of sulphidic diagenesis in non-bioturbated, shaly sediments. – *Org.*

944 *Geochem.,* **22**, 299–310.

945 WANG P. X., TIAN J. & LOURENS L. J. (2010). - Obscuring of long eccentricity

946 cyclicity in Pleistocene oceanic carbon isotope records. - *Earth and Planetary*

947 *Science Letters*, **290**, 3-4, 319-330.

948 WORDEN R.H. & BURLEY S.D. (2003). - Sandstone diagenesis: the evolution from

949 sand to stone. - *In:* S.D. Burley & R.H. Worden (Eds.), Clastic Diagenesis: Recent

950 and Ancient, International Association of Sedimentologists, **4**, 3–44.

951 WORDEN R. H. & MORAD S. (2003). - Clay minerals in sandstones: controls on

952 formation, distribution and evolution. - *In:* R.H. Worden & S. Morad (Eds.), Clay

953 mineral cements in Sandstones. Blackwell Publishing, 3-41.

954   ZIEGLER M., JILBERT T., DE LANGE G. J., LOURENS L. J. & REICHART G.-J.

955   (2008). - Bromine counts from XRF scanning as an estimate of the marine organic

956   carbon content of sediment cores. - *G-cubed*, **9**, Q05009.

957

958   Figure captions

959   Figure 1: Morphobathymetric map of the Nile margin and location of the studied core

960   MD04 2723.

961   Figure 2: Core MD04 2723 data evolution with age: lithology, isotopic stratigraphy,

962   Marine Isotopic Stages (MIS), Ca, BrTot, TOC and Sm%.

963   Figure 3: Modified van Krevelen diagram showing the sapropel results (N=20) with

964   indications of the sapropel number and TOC content in %.

965   Figure 4: The relationship between TOC and solid-phase bromine. Bromine data

966   values below the detection limit (5 ppm) were nullifying. Black dots: S5 sequence,

967   Black squares: S28 sequence, Black dash: other sequences.

968   Figure 5: Evolution of the BrOrg/TOC ratio with age by sapropelic sequence.

969   Time is obviously a factor in BrOrg variability. The evolution of the slope (or ratio of

970   BrOrg to TOC) with age indicates a loss of BrOrg of approximately 50% in 1.1 million

971   years.

972   Figure 6: Evolution of BrOrg with age by TOC range. Red crosses: <0.5%, purple

973   dots: 1.5-2.3%, blue triangles: 2.3-3% and green squares: 4.0-6.5%.

974   Figure 7: XRD patterns of the clay material extracted from sample MD04 2723 – 1 –

975   48. Diffractograms of the oriented preparations of the less than 2 µm fraction size

976   acquired in air-dried conditions (A.D.) and after saturation with ethylene glycol.

977

978   Figure 8: Aspect of the smectitic material in the middle part of the S5 sapropelic

979   horizon (section 6, 22.5-23.5 cm): (a) SEM observation, an intimate mixture of clay

980   and carbonaceous particles in the bulk material; (b) flakes of smectite particles

981 deposited onto a glass slide; (c) HRTEM image of the individual crystallites of the

982 smectite tactoids.

983

984 Figure 9: Decomposition of the near-infrared spectra of samples in which the clay

985 material is composed of (a) 75% smectite–25% kaolinite and (b) 90% smectite–10%

986 kaolinite. See Herbert et al., 2015 for more details on the method of quantification of

987 Sm%.

988 Figure 10: Main results through time, solid-phase organic bromine evolution as a

989 function of the TOC range (each straight line corresponds to a different

990 debromination rate), and relative stability of the detrital montmorillonite supply.

991

Figures

Figure 1

996
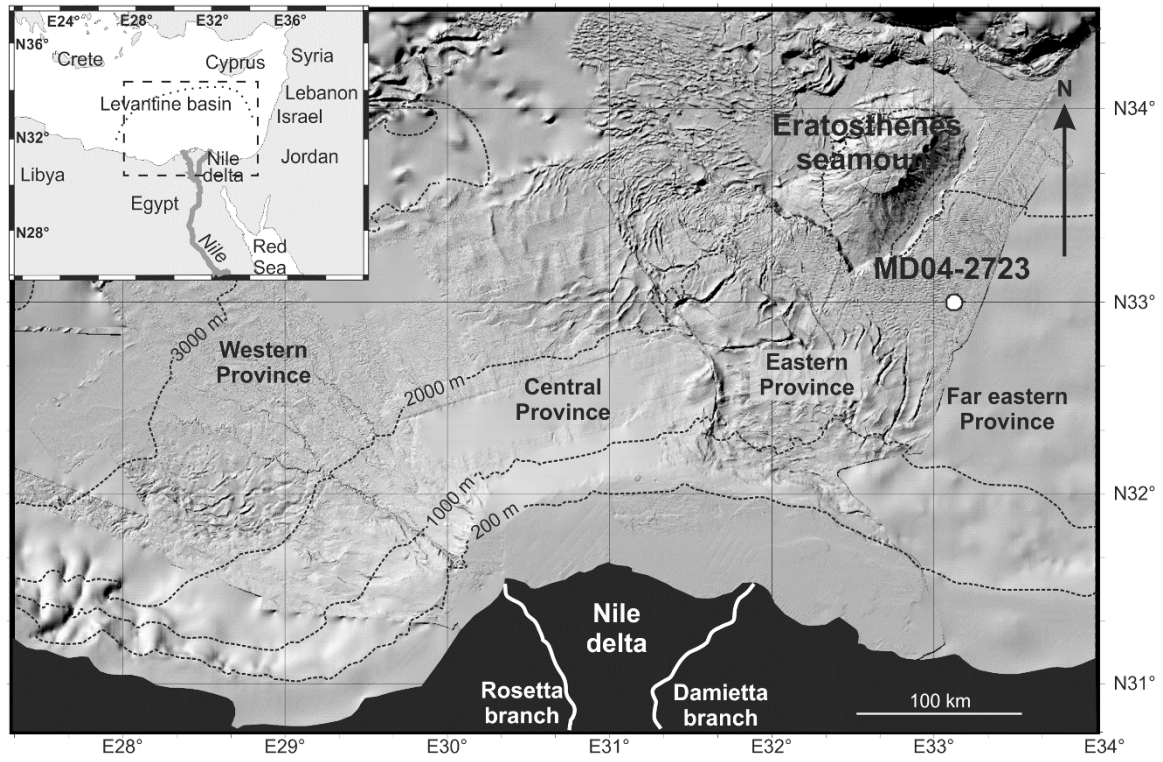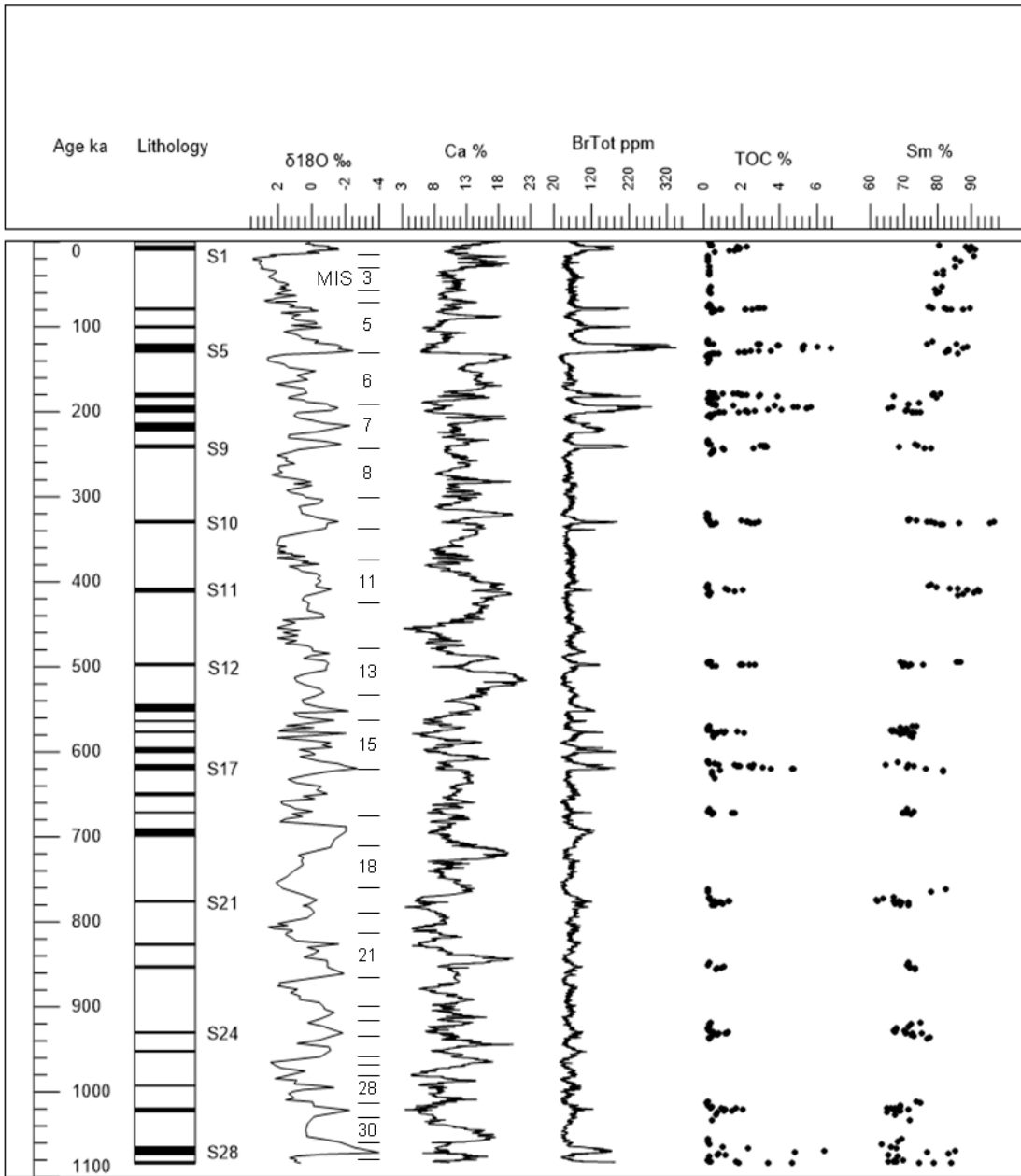
997
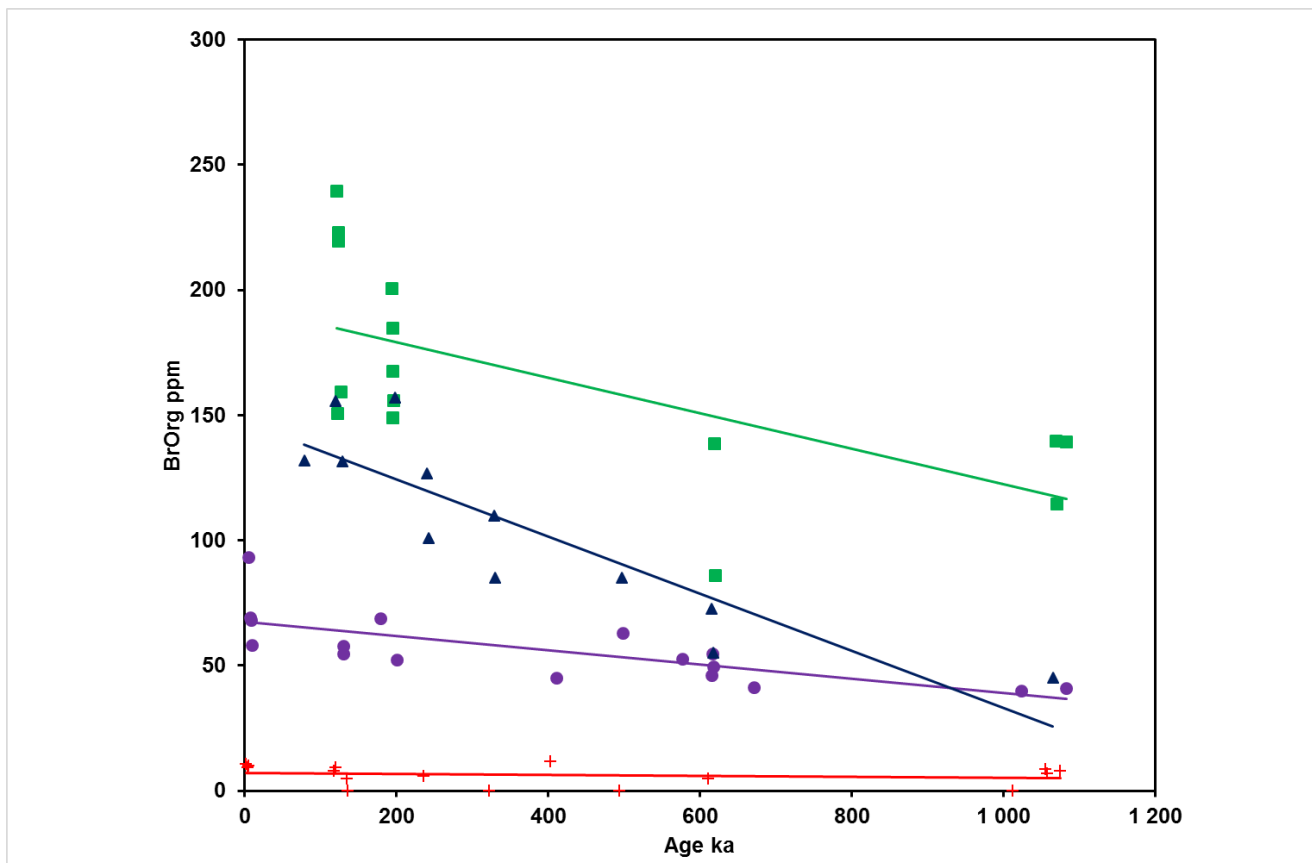998   Figure 2

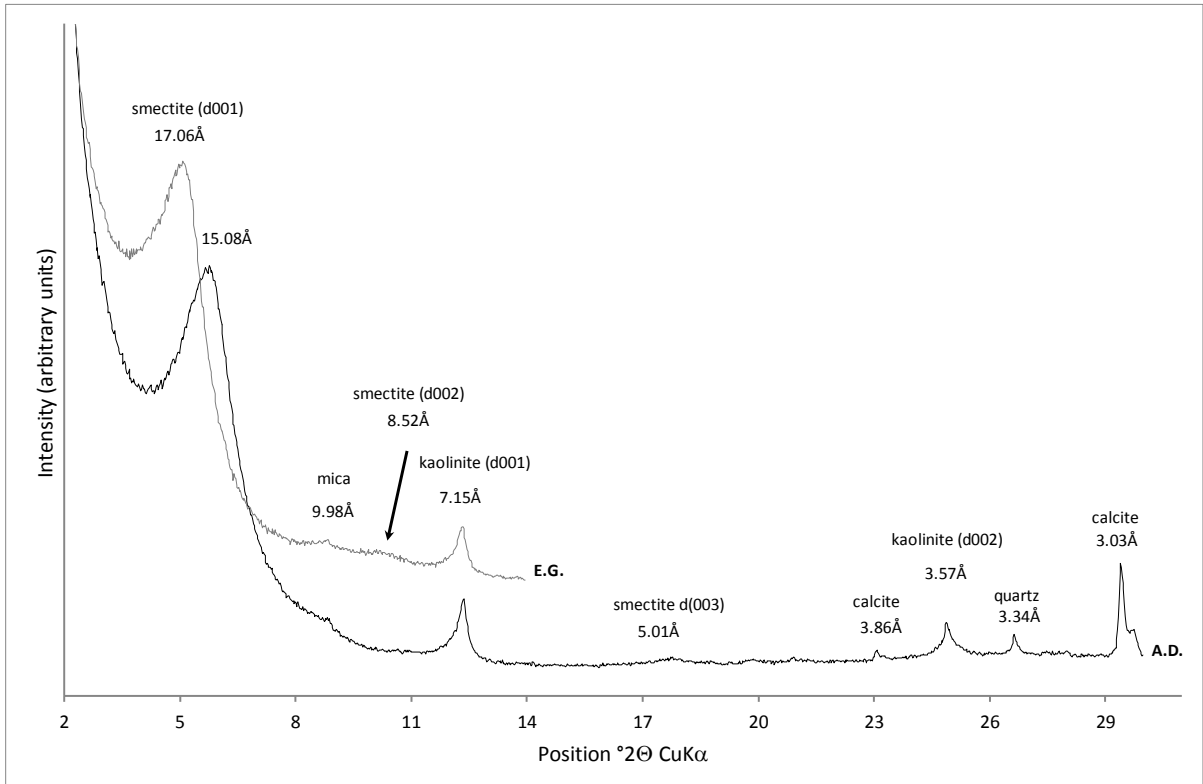999

45
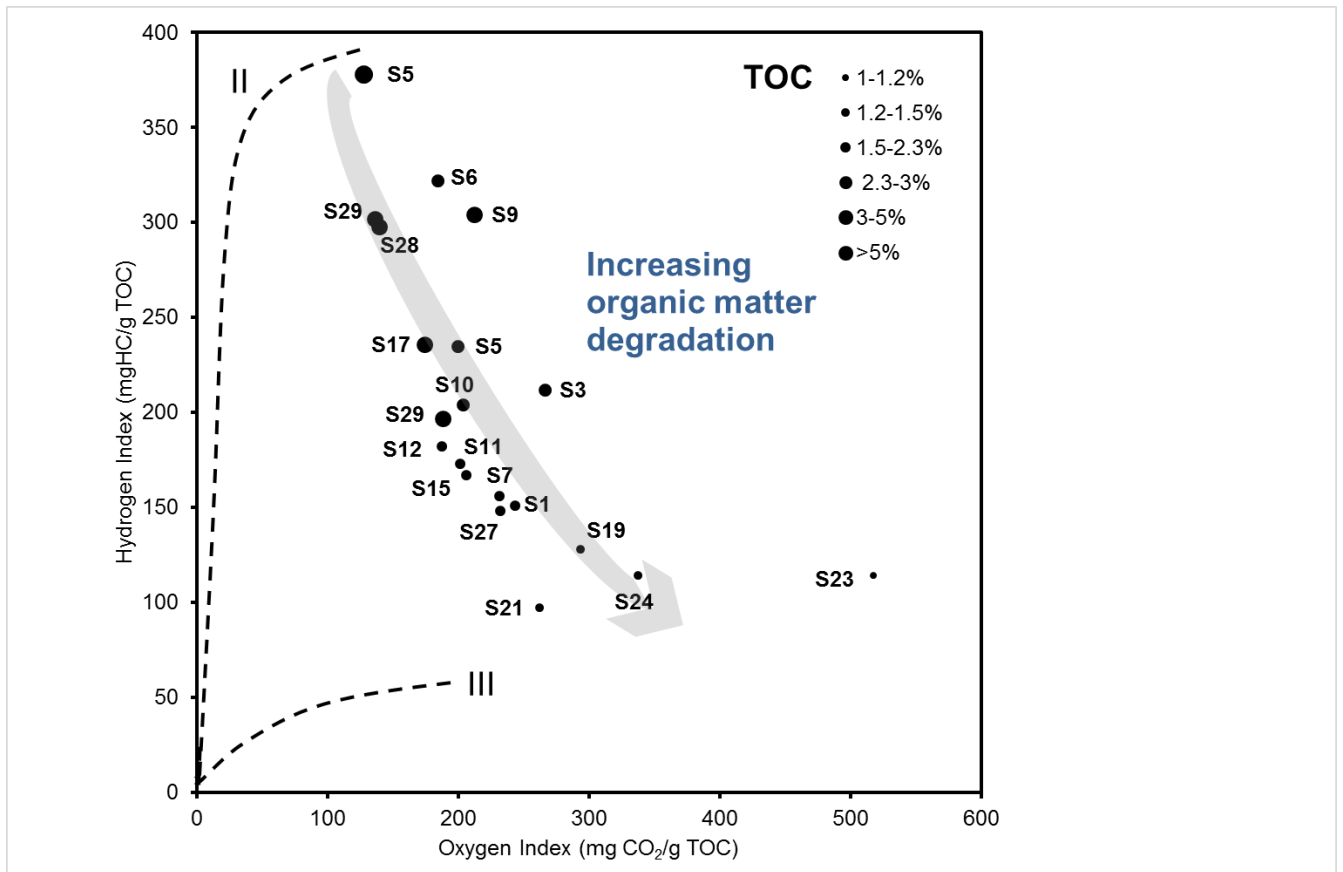
1000

1001   Figure 3
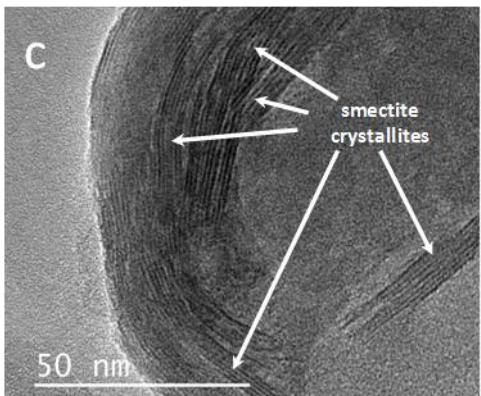
1002
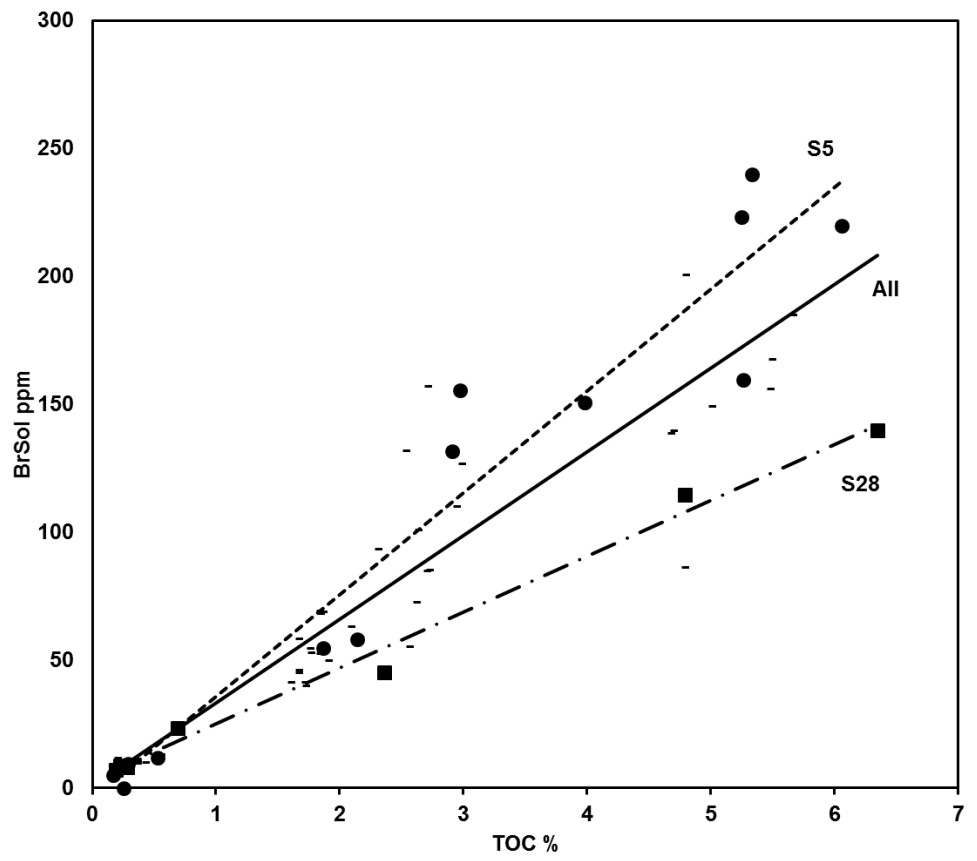
1003

1004   Figure 4
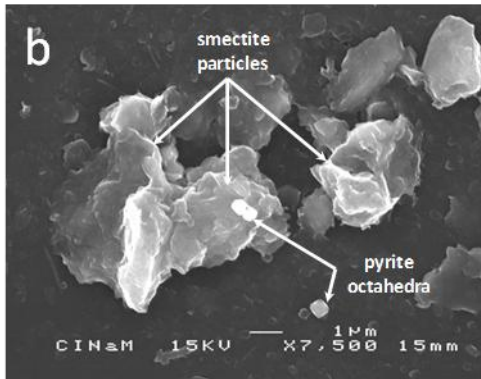
1005
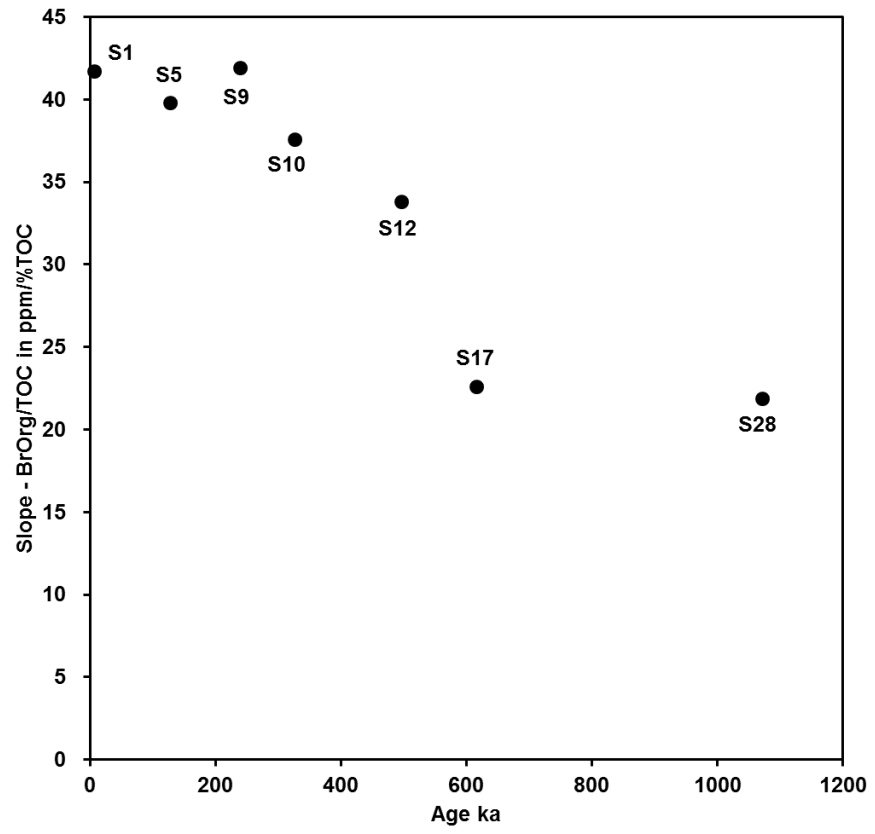
1006

1007 Figure 5

1008

1009

1010   Figure 6
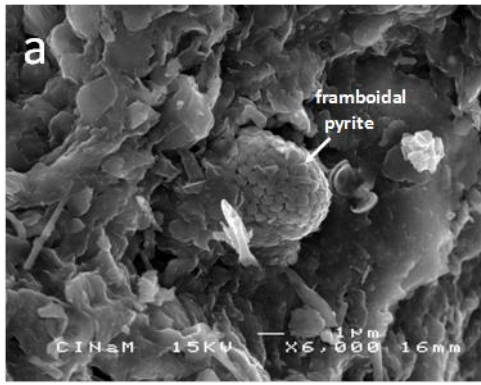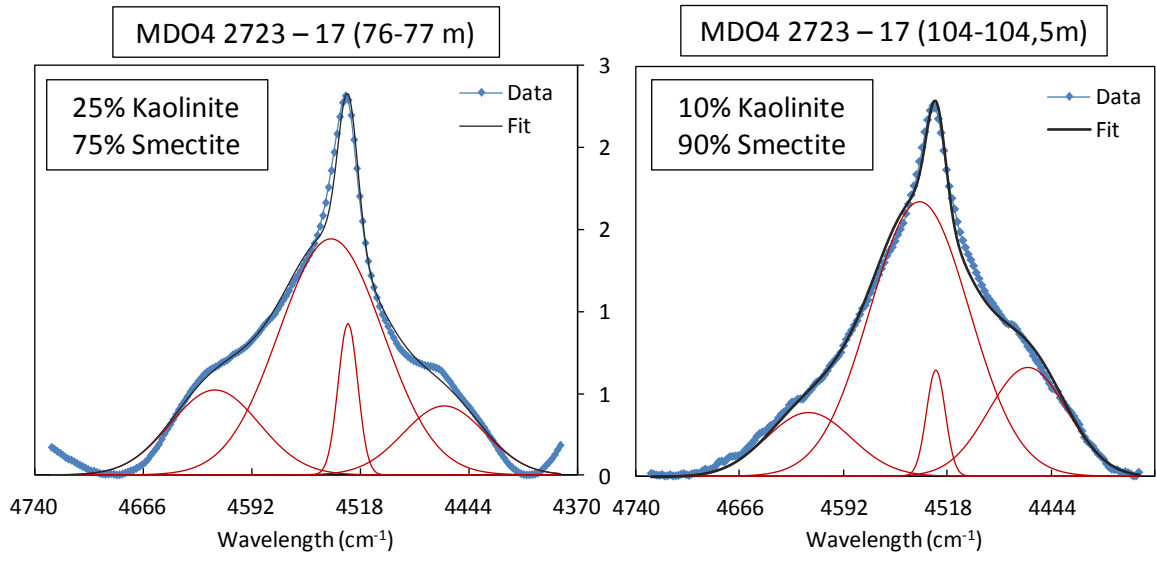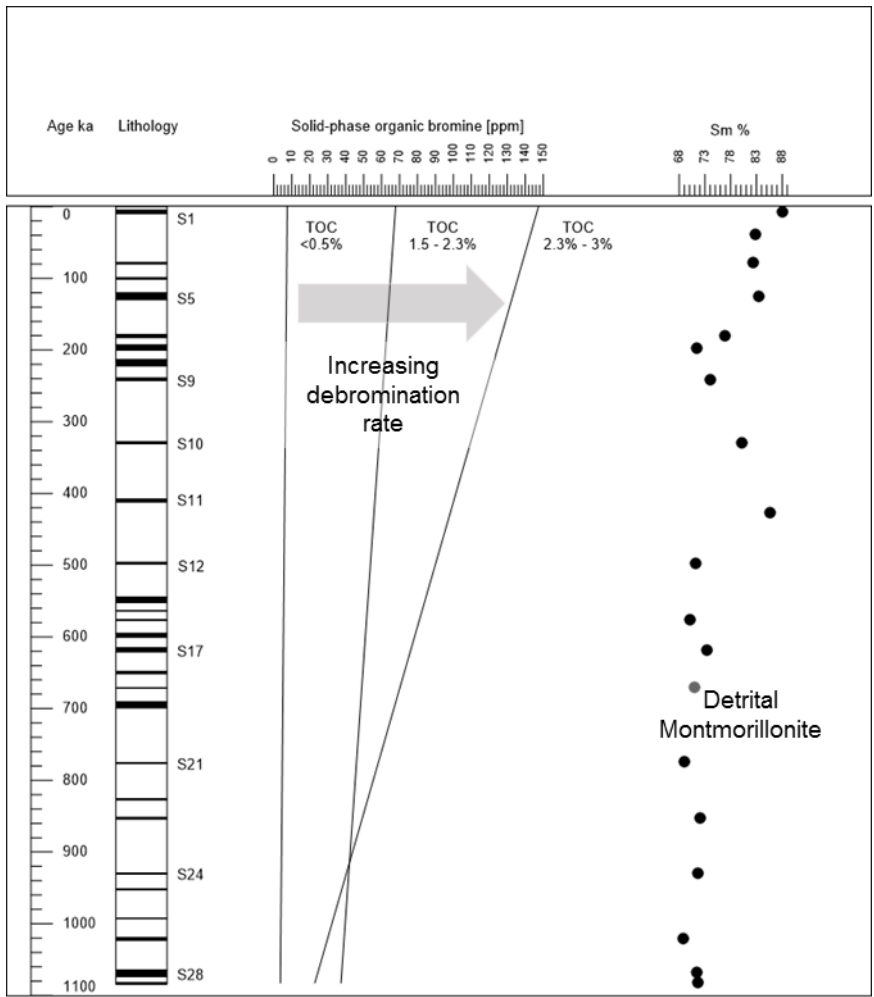
1011

1012

Figure 7

1014

1015

1016   Figure 8

1017

Figure 9

52

1021

1022   Figure 10

1023

1024   Table captions

1025   Table 1: Statistical results of the regression analysis of the TOC-BrOrg relationship.

1026 $p>0.05$ is non significant (NS), p between 0.05 and 0.01 is significant (S), p between

1027   0.01 and 0.001 is highly significant (HS), and $p<0.001$ is very highly significant

1028   (VHS). The slope corresponds to the ratio of BrOrg to TOC in ppm/%TOC.

1029   Table 2: Evolution of BrOrg with age by TOC range. Statistical results: $p>0.05$ is non

1030   significant (NS), p between 0.05 and 0.01 is significant (S), p between 0.01 and

1031   0.001 is highly significant (HS), and $p<0.001$ is very highly significant (VHS).

1032   Table 3: Representative structural formulas of smectite particles analyzed by TEM-

1033   EDX (1 and 2) and SEM-EDX(3-5). Number of ions calculated on the basis of 11

1034   oxygens (Fe arbitrarily considered as Fe^{3+}). Int. ch: interlayer charge.

1035

1036   Tables

Sequence	Age [ka]	N	r	r^2	p-value	Slope	Intercept
All data		63	0.922	0.851	VHS	32.8	0.44
S1	6.13	8	0.996	0.993	VHS	41.7	-6.83
S5	127.47	14	0.968	0.937	VHS	39.8	-3.90
S9	238.94	3	0.996	0.992	NS	41.9	-2.72
S10	326.65	3	0.991	0.982	NS	37.6	-7.51
S12	495.89	3	0.999	0.999	S	33.8	-6.86
S17	615.48	8	0.909	0.825	HS	22.6	7.06
S28	1071.57	7	0.995	0.990	VHS	21.9	3.13

1037

1038   Table 1

1039

TOC range	Mean TOC	N	r	r^2	p-value	Slope	Intercept	% of loss BrOrg in 1 m.y.	Debromination rate [μmolBrOrg molC^{-1} y^{-1}]
< 0.5%	0.24	16	-0.171	0.029	NS	-0.002	6.92	NS	NS
1.5 - 2.3 %	1.83	17	-0.736	0.542	HS	-0.028	67.53	41	2.3 10^{-4}
2.3 - 3.0 %	2.73	12	-0.878	0.771	HS	-0.115	147.46	78	6.3 10^{-4}
4.55 - 5.4%	4.95	9	-0.688	0.473	S	-0.087	201.34	43	2.6 10^{-4}
5.4 - 6.5%	5.80	5	-0.671	0.450	NS	-0.051	192.07	NS	NS
4.0 - 6.5 %	5.17	15	-0.640	0.410	S	-0.071	193.31	37	2.0 10^{-4}

1040

1041   Table 2

1042

	1	2	3	4	5
Si	3.97	3.83	3.91	3.91	3.84
Al^{IV}	0.03	0.17	0.09	0.09	0.16
Al^{VI}	1.24	1.14	1.35	0.88	1.45
Fe^{3+}	0.31	0.26	0.28	0.53	0.26
Mg	0.53	0.65	0.37	0.59	0.29
Ca	0.09	0.17	0.03	0.05	0.14
Na	0.10	0.17	0.25	0.31	0.12
K	0.06	0.14	0.14	0.26	0.07
Int. Ch.	0.35	0.65	0.45	0.67	0.47

1043

1044   Table 3